S TRANSFORM :
TIME FREQUENCY ANALYSIS & FILTERING

A Thesis submitted in partial fulfillment
of the requirements for the degree of

Master of Technology

in

Telematics and Signal Processing

by

NITHIN V GEORGE
ROLL NO : 207EC107

Department of Electronics and Communication Engineering
National Institute of Technology
Rourkela, India
2009

S TRANSFORM :
TIME FREQUENCY ANALYSIS & FILTERING

A Thesis submitted in partial fulfillment
of the requirements for the degree of

Master of Technology

in

Telematics and Signal Processing

by

NITHIN V GEORGE
ROLL NO : 207EC107

under the guidance of

Dr. G. PANDA

Department of Electronics and Communication Engineering
National Institute of Technology
Rourkela, India
2009

National Institute of Technology

Rourkela

CERTIFICATE

This is to certify that the thesis entitled, **" S Transform : Time Frequency Analysis and Filtering "** submitted by **Nithin V George** in partial fulfillment of the requirements for the award of Master of Technology Degree in **Electronics & Communication Engineering** with specialization in **Telematics and Signal Processing** during 2008-2009 at the National Institute of Technology, Rourkela (Deemed University) is an authentic work carried out by him under my supervision and guidance.

To the best of my knowledge, the matter embodied in the thesis has not been submitted to any other University / Institute for the award of any Degree or Diploma.

Date

Prof. G. Panda (FNAE, FNASc)

Dept. of Electronics & Communication Engg.

National Institute of Technology

Rourkela-769008

Orissa, India

Acknowledgements

I am deeply indebted to **Dr. G. Panda**, my supervisor on this project, for consistently providing me with the required guidance to help me in the timely and successful completion of this project. In spite of his extremely busy schedules, he was always available to share with me his deep insights, wide knowledge and extensive experience. His advices have value lasting much beyond this project. I consider it a blessing to be associated with him.

The completion of the research work that culminates into this thesis wouldn't have been possible without the able guidance of **Dr. Lalu Mansinha** of the University of Western Ontario, London, Canada. I consider myself highly fortunate to have received the opportunity to learn from this erudite and equanimous teacher. Although he was not part of the UWO faculty, he had spared substantial amount of his personal time for me and gave me the required inputs, advices and assistance. I would like to gratefully acknowledge all his support and guidance.

I also owe many thanks to **Dr. Kristy F Tiampo** of the University of Western Ontario, London, Canada who had supervised my project work at UWO. The energy and effectiveness inherent in all her involvement had been amazing. I would consider her a role model for anyone aspiring to be successful in life. I am also grateful to the University of Western Ontario, London, Canada for granting me the required access to the resources available at the department of Earth Sciences.

I was also the beneficiary of essential advice and assistance of the faculty and staff at NIT Rourkela. I gratefully acknowledge the kindness and cooperation extended to me specially by **Dr.S.K.Patra** (Head, Department of Electronics and Communication Engineering), **Dr.G.S.Rath**, **Dr.K.K.Mahapatra**, **Dr.S.Meher**, **Dr.S.K.Behera** , **Dr.D.P.Acharya** and **Prof.A.K.Sahoo** . I also remember with gratitude my friends who have been always available at hand to motivate, encourage and help me out.

Finally I would like to thank the Department of Foreign Affairs and International Trade (DFAIT), Govt. of Canada, for the scholarship granted to me that had provided me the financial support to successfully complete my assignments under the Graduate Student Exchange Programme (GSEP) fellowship at the University of Western Ontario, London, Canada.

Nithin V George

Contents

Abstract

The S transform, a hybrid of the Short Time Fourier Transform and Wavelet transform, has a time frequency resolution which is far from ideal. This thesis proposes a modified S transform, which offers better time frequency resolution compared to the original S transform. The improvement is achieved through the introduction of a new scaling rule for the Gaussian window used in S transform. The S transform analysis of financial time series revealed the presence of business cycles, which could help forecasting economic booms and recessions. A noisy time series, with both signal and noise varying in frequency and in time, presents special challenges for improving the signal to noise ratio. The modified S-transform time-frequency representation is used to filter a synthetic time series in a two step filtering process. The filter method appears robust within a wide range of background noise levels. The new filtering approach developed was successfully applied for the identification of Post Glacial rebound in Eastern Canada.

List of Figures

List of Tables

List of Acronyms

FT	Fourier Transform
STFT	Short Time Fourier Transform
WT	Wavelet Transform
CWT	Continuous Wavelet Transform
DWT	Discrete Wavelet Transform
TFR	Time Frequency Representation
LTV	Linear Time Varying
ST	Stockwell Transform
GDP	Gross Domestic Product
GPS	Global Positioning System
NS	North South
EW	East West
GIA	Glacial Isostatic Adjustment
GMT	Generic Mapping Tools
TV	Time Variance

1

Introduction

A time series is a sequence of data points, measured typically at successive times. A time series $x(t)$, $t = 1, 2, \ldots$ is called a stationary time series if its statistical properties do not change with time t. Spectral Analysis using the Fourier transform is a powerful tool for stationary time series analysis. But for non-stationary time series, the statistical properties changes with time and hence the time averaged amplitude spectrum obtained using Fourier transform is inadequate to track the changes in the signal magnitude, frequency or phase. The advent of time frequency analysis techniques using Short Time Fourier Transform (STFT) and Wavelet Transform made the analysis of non stationary signals simpler. The fixed resolution of the STFT and the absence of phase information in the Wavelet transform led to the development of the S transform, which retains the absolute phase information, in the mean while, have good time frequency resolution for all frequencies. Even though the S transform has better time frequency resolution compared to STFT, the resolution if far from ideal. The resolution needs improvement.

Integrating the S transform over time results in the Fourier transform. This direct relation to the Fourier transform makes the inversion to time domain an easy task. This property of the S transform led to the development of S transform filters, which uses an analysis-weighting-synthesis procedure. The extra time dimension in the time frequency filters gives the designer an enhanced opportunity to clearly define the pass bands and stop bands. Current literature on time frequency filters using S transform uses a regular shaped pass band or stop band (e.g. Rectangular), which makes the filtering intricate when the signal and the noise exists in an irregular intermixed pattern in the time frequency domain.

The objective of this work is to improve the time frequency resolution of S transform, develop a simple in-band filtering approach using S transform and to use the filtering technique for analysis of Geophysical time series. The thesis is organized as follows.

Chapter 2 gives an introduction to time series analysis. It also includes a brief review of the signal processing tools like the Fourier transform, Short Time Fourier transform and the Wavelet transform. The short comparison between the advantages and disadvantages of each method is presented.

Chapter 3 presents the S transform, which is a new time frequency analysis technique. A modified S transform is proposed , which has better time frequency resolution compared to the original S transform. The improvement in resolution is demonstrated using a set of synthetic time series.

In Chapter 4, the S transform is used for the analysis of Business cycles. Stock price indices are used as an indicator of the business cycles. Valuable information that are

obvious neither from the time series nor from the Fourier analysis of business data are obtained using S transform time frequency analysis.

A novel time frequency filtering approach is introduced in Chapter 5. Image processing algorithms are combined with S transform to perform filtering of noisy time series, with both signal and noise varying in frequency and in time. The filtering procedure is validated using synthetic signals.

The time frequency filtering procedure introduced in Chapter 5, is applied to real data in Chapter 6. In Chapter 6, time frequency filters are applied to filter Global Positioning System (GPS) time series collected for Eastern Canada. The study reveals the presence of a post glacial rebound. The results are in close match with the Post Glacial Rebound models for Eastern Canada.

Conclusions are drawn in Chapter 7. Future work has also been discussed in this chapter.

2

Time Series Analysis

2.1 Introduction

A time-series is a set of data recorded over a length of time. It is normally an output of a measuring instrument. Most time series patterns can be described in terms of two basic classes of components: trend and seasonality. Trend is a general systematic linear or nonlinear component that changes over time and does not repeat or at least does not repeat within the time range of the time series. Seasonality is similar to trend but it repeats itself in systematic intervals over time. These two general classes of time series components may coexist in real-life data.

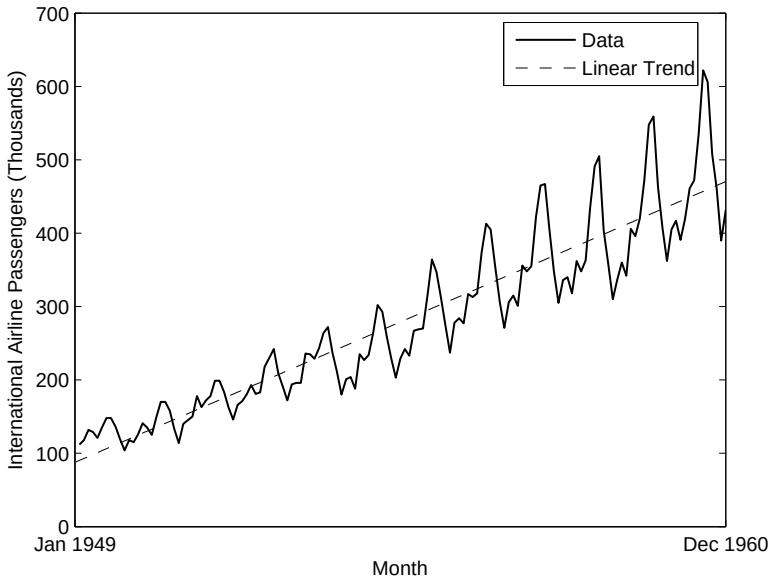

Figure 2.1: Series 'G'

The two components of a time series are clearly visible from the G series [1],which shows the monthly international airline passenger totals (measured in thousands) in twelve consecutive years from 1949 to 1960. The plot shows a clear linear trend which shows that there was an obvious growth of airline passengers with year. The monthly figures follow an almost identical pattern each year, which refers to the seasonality factor. i.e. More people travel during vacations.

2.2 Trend Analysis

There is no well laid out rule or technique to calculate trend in a time series. If the trend is either a monotonically increasing or decreasing one, its computation may not be difficult. If the time series data contain considerable error, then the first step in the process of trend identification is smoothing. Smoothing normally involves a form of local averaging of data such that the non systematic components of simultaneous observations cancel each other out. The most common technique is moving average smoothing which replaces each element of the series by either the simple or weighted average of N surrounding elements, where N is the width of the smoothing 'window' [1]. Medians can be used instead of means. The main advantage of median as compared to moving average smoothing is that its results are less biased by outliers (within the smoothing window). Thus, if there are outliers in the data, median smoothing typically produces smoother curves than moving average based on the same window width. The main disadvantage of median smoothing is that in the absence of clear outliers it may produce more 'jagged' curves than moving average and it does not allow for weighting. A normal trend identification involves a lower order polynomial, exponential or logarithmic curve fitting to the time series after removing non linear components by smoothing.

2.3 Seasonality Analysis

Seasonality is defined as correlational dependency of order k between each ith element of the series and the $(i-k)$th element and measured by autocorrelation. The parameter k is usually called the lag. If the time series is devoid of outliers and large measurement errors, seasonality can be visually identified in the series as a pattern that repeats every k elements. The seasonality of a time series can be analyzed using a correlogram, which displays graphically and numerically the autocorrelation function , that is, serial correlation coefficients for consecutive lags in a specified range of lags. Serial dependency for a particular lag of k can be removed by differencing the series, that is converting each ith element of the series into its difference from the $(i-k)$th element. There are two major reasons for such transformations. First, one can identify the hidden nature of seasonal dependencies in the series. The second reason for removing serial dependency is to make the time series stationary (constant mean, variance, and autocorrelation through out the full length of the time series).

2.4 Spectral Analysis

Spectral Analysis is a third type of analysis that can be done on a time series. It is used to study the cyclic nature of a time series apart from the seasonality.

2.4.1 Fourier Transform

Fourier Transform is one of most common spectral analysis technique. It transforms a time domain signal to a frequency domain signal, which is an alternate representation of a signal. In most cases the frequency domain shows certain features of the signal that were not visible in the time domain. Fourier transform changes the delta basis function in the time domain to infinitely long sinusoidal basis functions in the frequency domain. The sinusoidal basis functions are the solutions to the mathematical equation describing a small perturbation of a physical system about a stable equilibrium point [2].

The Fourier transform $X(f)$ of a time series $x(t)$ is given by

$$X(f) = \int_{-\infty}^{\infty} x(t) e^{-i2\pi ft} dt \tag{2.1}$$

and its inverse relationship is given by

$$x(t) = \int_{-\infty}^{\infty} X(f) e^{i2\pi ft} df \tag{2.2}$$

The discrete version of the Fourier Transform called the Discrete Fourier Transform (DFT) of a time series of length N is given by

$$X\left[\frac{n}{NT}\right] = \frac{1}{N} \sum_{k=0}^{N-1} x(kT) e^{-\left(\frac{i2\pi nk}{N}\right)} \tag{2.3}$$

where T is the sampling interval of the time series. The inversion relationship is

$$x(kT) = \sum_{n=0}^{N-1} X\left[\frac{n}{NT}\right] e^{\left(\frac{i2\pi nk}{N}\right)} \tag{2.4}$$

Study of the function $[X(f)]^2$ is called Periodogram Analysis. Even though Fourier transform can estimate all integer frequencies to a certain extend, it has several disadvantages :

- Fourier Transform cannot estimate fractional frequencies. The Fourier Transform of signals with fractional frequencies, results in spreading of the spectrum to other

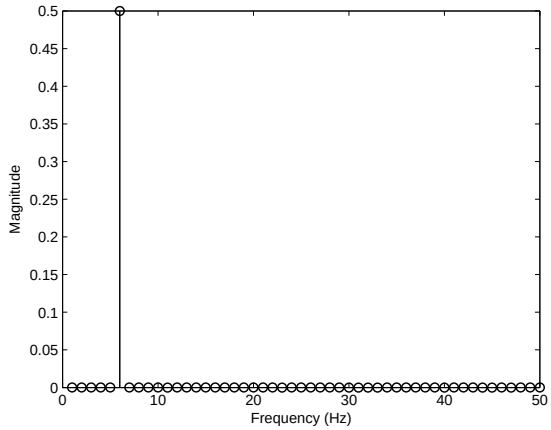

(a) Amplitude Spectrum of 5Hz sinusoidal time-series

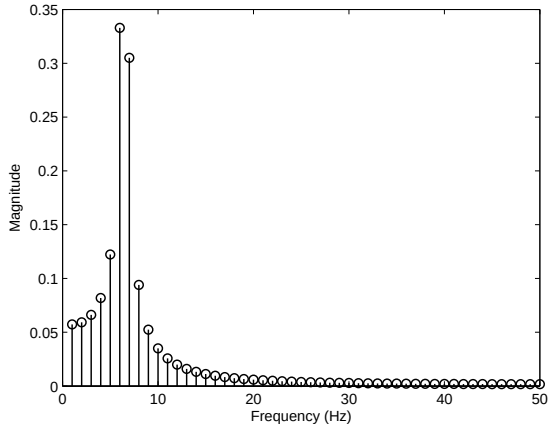

(b) Amplitude Spectrum of 5.5Hz sinusoidal time-series

Figure 2.2: Fourier Amplitude Spectrum : Fractional Frequencies

frequencies that are not actually present in the original time-series (Figure 2.2).

- For non stationary time series, the spectral content changes with time and hence the time averaged amplitude spectrum computed using Fourier Transform is inadequate to track the changes. No information can be induced from the Fourier Amplitude spectrum on when a particular frequency components exists in a signal (Figure 2.3,2.4). The time information of the spectral elements are hidden in the phase spectrum.

- If a particular frequency signal exists for a very small duration in a long time series, the short duration frequency will not be noticeable in the amplitude spectrum (Figure 2.5).

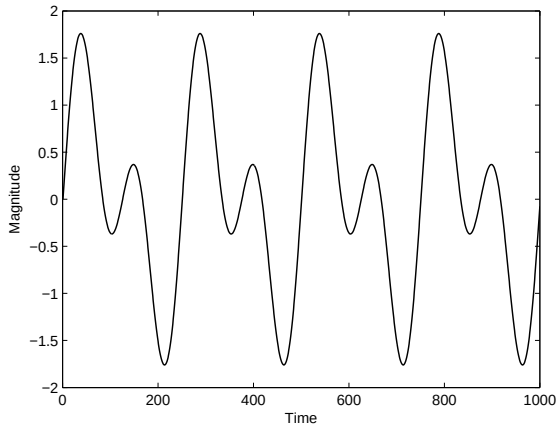

(a) A 4Hz sinusoidal time-series added with an 8Hz sinusoidal time-series

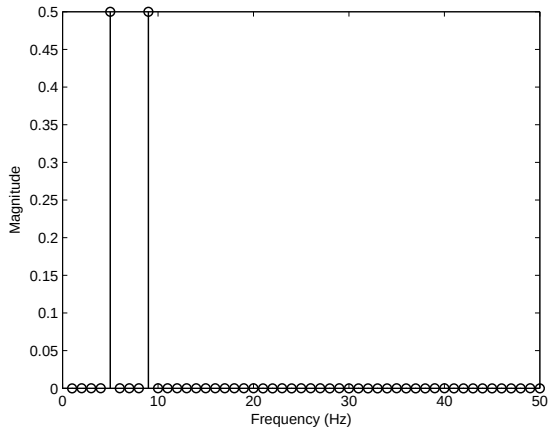

(b) Amplitude Spectrum of the above time series

Figure 2.3: Fourier Amplitude Spectrum : Stationary Signal

The solution to most of the above mentioned difficulties of Fourier Transform is the Time-Frequency spectral analysis.

2.4.2 Short Time Fourier Transform(STFT)

STFT was one of the first Time-Frequency representation technique. It multiplies the time series with a series of shifted time windows and calculates the Fourier transform of that multiplied signal [3]. STFT of a signal $x(t)$ is given by:

$$STFT(\tau, f) = \int_{-\infty}^{\infty} x(t)w(t-\tau)e^{-i2\pi ft}dt \tag{2.5}$$

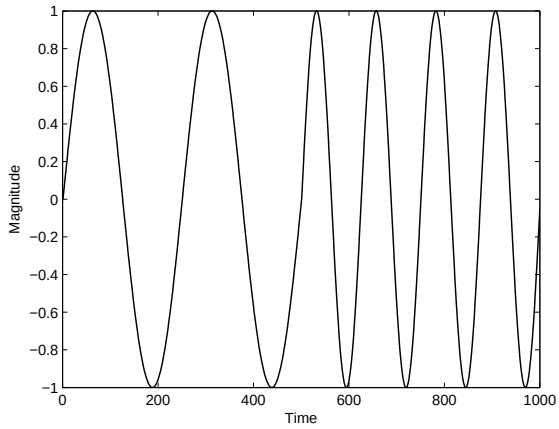

(a) Time series with 4Hz sinusoidal for first 500 samples and with an 8Hz sinusoidal for the next 500 samples

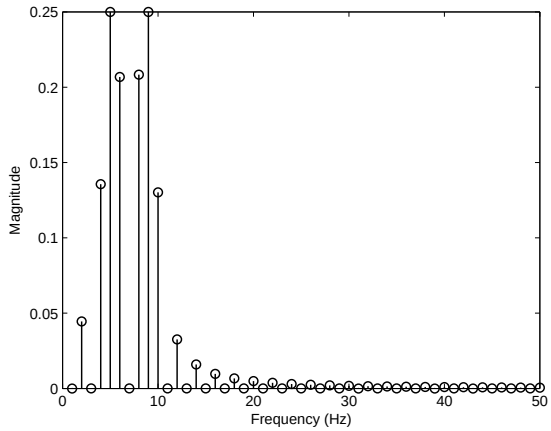

(b) Amplitude Spectrum of the above time series

Figure 2.4: Fourier Amplitude Spectrum : Non Stationary Signal

where $w(t)$ is an arbitrarily chosen window function. The window size is chosen in such a way to make sure that the windowed signal segment can be assumed to be stationary. The windowing results in a localization in time and hence the spectrum thus obtained is called a local spectrum. This localizing window is moved in time along the entire length of the time series and localized spectrum is calculated. The 2D representation of this spectrum is called Spectrogram.

Time resolution is defined as how well a transform can resolve rapid variations in the time domain and frequency resolution refers to how well the changes in frequencies of a signal can be tracked. The time and frequency resolution are dependent directly on the width of the window used in time frequency analysis. Frequency resolution is proportional

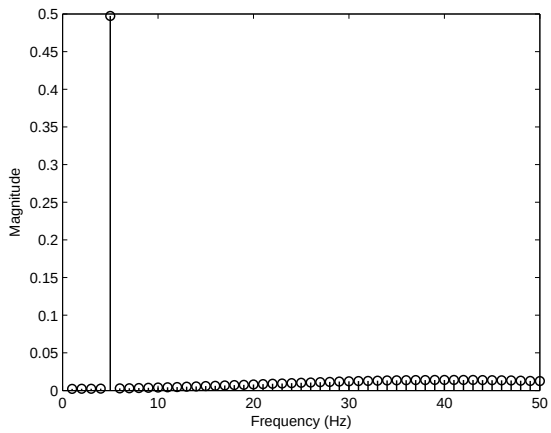

Figure 2.5: Amplitude Spectrum of a 4Hz sinusoidal signal of 1000 samples with a 40Hz signal for a short duration of 30 samples

to the bandwidth of the windowing function while time resolution is proportional to the length of the windowing function. Thus a short window is needed for good time resolution and a wider window offers good frequency resolution.

The limitation of the time frequency resolution is due to the Heisenberg-Gabor inequality that states that

$$\Delta t.\Delta f \geq K \tag{2.6}$$

where Δt is the time resolution, Δf is the frequency resolution and K is a constant that depends on the type of window used. Therefore to attain good time resolution as well as frequency resolution, one has to go for a pair of STFT, one with a narrow window (which gives good time resolution) and another with a wider window (good frequency resolution). Figure 2.6(a) shows a test time series, which contains three frequencies. The first 64 samples of the time series have a frequency of 6Hz, the next 64 samples are of a frequency of 25Hz. A short duration signal of 52Hz have been added to the samples from 20 to 30. The three different frequencies are visible in the time frequency representation (Figure 2.6(b)) obtained using STFT. The window used is a Gaussian window with a standard deviation of 8. The frequency resolution is not good for the lower frequency signal components and the short duration high frequency signal does not have a good energy concentration.

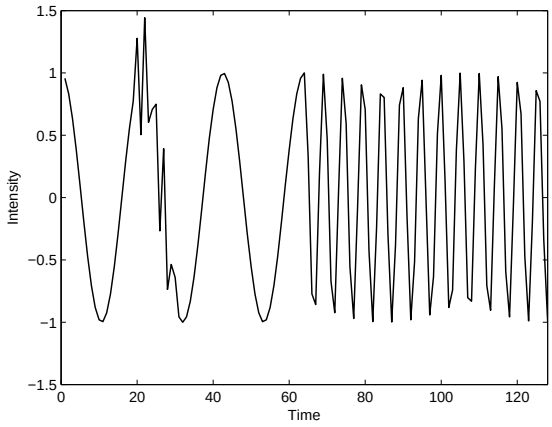

(a) Test time series

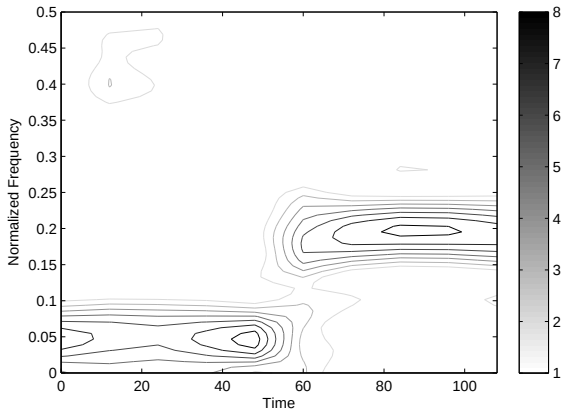

(b) Short Time Fourier Transform : Test Series

Figure 2.6: Short Time Fourier Transform

2.4.3 The Wavelet Transform

A wavelet is a continuous time signal that satisfies the following properties

$$\int_{-\infty}^{\infty} \psi(t)dt = 0 \tag{2.7}$$

$$\int_{-\infty}^{\infty} |\psi(t)|^2 \, dt < \infty \tag{2.8}$$

where $\psi(t)$ is defined as the mother wavelet [4]. The continuous wavelet transform

$$W(a,b) = \int_{-\infty}^{\infty} y(t)\psi^*_{a,b}(t)dt \tag{2.9}$$

where $y(t)$ is any square integrable function,a is the dilation parameter, b is the translation parameter and $\psi^*_{a,b}(t)$ is the dilation and translation(asterik denotes the complex conjugate) of the mother wavelet defined as

$$\psi^*_{a,b}(t) = \frac{1}{\sqrt{|a|}}\psi\left(\frac{t-b}{a}\right) \tag{2.10}$$

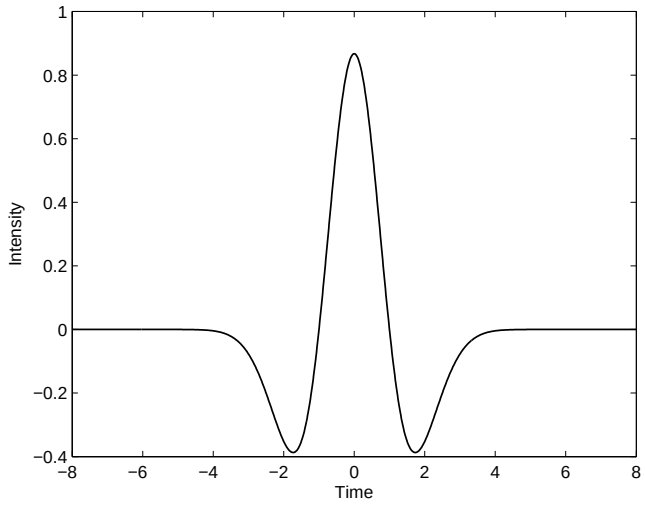

Figure 2.7: Mexican Hat Wavelet

The signal $y(t)$ can be reconstructed from the continuous wavelet transform provided the mother wavelet satisfies the admissibility condition,

$$C = \int_{-\infty}^{\infty} \frac{|\Psi(\omega)|^2}{|\omega|}dw < \infty \tag{2.11}$$

where $\Psi(\omega)$ is the Fourier Transform of $\psi(t)$. The reconstructed signal $y(t)$ is given as

$$y(t) = \frac{1}{C}\int_{a=-\infty}^{\infty}\int_{b=-\infty}^{\infty} \frac{1}{|a|^2}W(a,b)\psi_{a,b}(t)dadb \tag{2.12}$$

The Continuous Wavelet transform (CWT) is two dimensional. It is obtained by the inner product of the signal and dilations and translations of the mother wavelet. CWT is represented as a time scale plot, where scale is the inverse of frequency. At a

low scale (high frequency), CWT offers high time resolution and at higher scales (lower frequencies) CWT gives high frequency resolution. The interpretation of the time scale representations produced by the wavelet transform require the knowledge of the type of the mother wavelet (e.g. Mexican Hat (Figure 2.7),Gaussian etc.) used for the analysis. Thus the visual analysis of the wavelet transform is intricate.

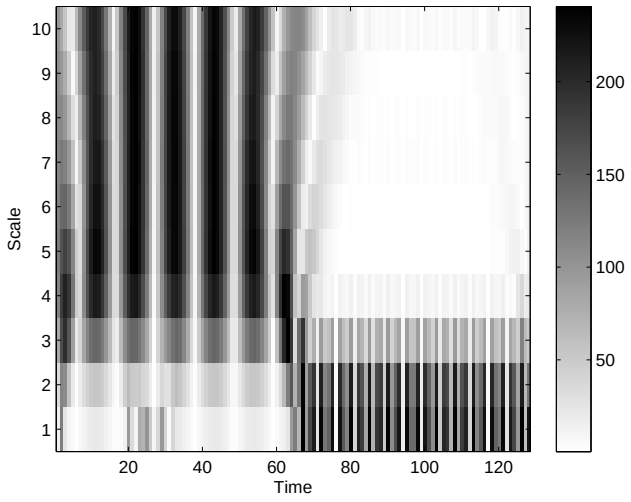

Figure 2.8: The Wavelet Transform

Figure 2.8 shows the time frequency representation of the test series (Figure 2.6(a)) using a Gaussian mother wavelet with scales 1 to 10. The short duration 52Hz signal is visible as a disturbance at the lower scales. The other two signals can be identified but direct reading of the frequency of the signal as well as its frequency components from the time scale plot is difficult.

2.5 Discussion

Frequency analysis of signals gives information about the signals that cannot be inferred from the time domain signal. Fourier spectral analysis is a good tool for stationary signal analysis. But when the signal has time varying statistical parameters, the signals need to be analyzed in time frequency domain. STFT and Wavelet transforms are two candidates for time frequency analysis. STFT has fixed time frequency resolution and the interpretation of the time scale plots obtained in Wavelet transforms are difficult to interpret.

3

Modified S Transform

3.1 Introduction

The field of time frequency analysis got an impetus with the development of the Short Time Fourier Transform (STFT). The STFT is a localized time frequency representation of a time series. It uses a windowing function to localize the time and the Fourier transform to localize the frequency. On account of the fixed width of the window function used, STFT has poor time frequency resolution. The Wavelet Transform (WT) on the other hand uses a basis function which dilates and contracts with frequency. The WT does not retain the absolute phase information and the visual analysis of the time scale plots that are produced by the WT is intricate. A time frequency representation developed by Stockwell [5], which combines the good features of STFT and WT is called the S transform. It can be viewed as a frequency dependent STFT or a phase corrected Wavelet transform.

3.2 Stockwell Transform

Given a time series $h(t)$, the local spectrum at time $t = \tau$ can be determined by multiplying $h(t)$ with a Gaussian located at $t = \tau$. Thus the 'Stockwell Transform [1]' is given by

$$S(f, \tau, \sigma) = \int_{-\infty}^{\infty} h(t) g(t - \tau) e^{-i2\pi ft} dt \tag{3.1}$$

The most convenient way of looking at the integral is to define

$$p_1(t, f) = h(t) e^{-i2\pi ft} \tag{3.2}$$

Substituting in (3.1), we get

$$S(f, t, \sigma) = \int_{-\infty}^{\infty} p_1(t, f).g(t - \tau) dt \tag{3.3}$$

$$= p_1(t, f) * g(t, \sigma) \tag{3.4}$$

[1]Lecture notes on Stockwell Transform : Dr. Lalu Mansinha, The University of Western Ontario, Canada.

where $*$ denote the convolution operation. Let $S(f,\tau,\sigma) \leftrightarrow B(f,\alpha,\sigma)$, where $B(f,\alpha,\sigma)$ is the Fourier transform of $S(f,\tau,\sigma)$. Thus

$$S(f,\tau,\sigma) = \int_{-\infty}^{\infty} B(f,\alpha,\sigma) e^{-i2\pi\alpha\tau} d\alpha \tag{3.5}$$

From convolution theorem, we know that

$$\{p_1(t,f) * g(t,\sigma)\} \leftrightarrow \int_{-\infty}^{\infty} P_1(f,\alpha) e^{-2\pi\alpha t} d\alpha \tag{3.6}$$

Since $p_1(f,t) = h(t).e^{i2\pi ft}$,

$$P_1(f,\alpha) = H(\alpha) * \delta(\alpha - f) \tag{3.7}$$

$$B(f,\alpha,\sigma) = [H(\alpha) * \delta(\alpha - f)] .G(\alpha,\sigma) \tag{3.8}$$

$$S(f,\tau,\sigma) = \int_{-\infty}^{\infty} \{[H(\alpha) * \delta(\alpha - f)] .G(\alpha,\sigma)\} e^{-i2\pi\alpha\tau} d\alpha \tag{3.9}$$

$$B(f,\alpha,\sigma) = \int_{-\infty}^{\infty} S(f,\tau,\sigma) e^{i2\pi\alpha\tau} d\tau \tag{3.10}$$

$$B(f,\alpha,\sigma) = [H(\alpha) * \delta(\alpha - f)] .G(\alpha,\sigma) \tag{3.11}$$

$$[H(\alpha) * \delta(\alpha - f)] = \frac{B(f,\alpha,\sigma)}{G(\alpha,\sigma)} \tag{3.12}$$

Since $H(\alpha) * \delta(\alpha - f)$ is the forward translation of $H(\alpha)$, we can perform a backward translation to recover $H(\alpha)$ from $H(\alpha) * \delta(\alpha - f)$.

$$H(\alpha) * \delta(\alpha - f) = H(\alpha - f) \tag{3.13}$$

$$H(\alpha - f) = \frac{B(f,\alpha,\sigma)}{G(\alpha,\sigma)} \tag{3.14}$$

$$H(\alpha - f) * \delta(\alpha, f) = \left[\frac{B(f,\alpha,\sigma)}{G(\alpha,\sigma)}\right] * \delta(\alpha + f) \tag{3.15}$$

$$H(\alpha) = \frac{B(f,\alpha+f,\sigma)}{G(\alpha+f,\sigma)} \tag{3.16}$$

Therefore $S(f,\tau,\sigma)$ is the transform of $h(t)$ at $t = \tau$ and σ represents the width of the Gaussian $g(t)$. The sequence of operations for the calculation of S transform is

1. Determine

$$H(\alpha) \leftrightarrow h(t)$$
$$G(\alpha, \sigma) \leftrightarrow g(t, \sigma)$$

2. Calculate $H(\alpha) * \delta(\alpha - f)$, which is $H(\alpha)$ translated to f.

3. Multiply $G(\alpha, \sigma)$ and shifted $H(\alpha)$

4. Take the inverse Fourier Transform

For the original S transform, Stockwell and Mansinha made σ, the dilation parameter a function of frequency f.

$$\sigma = \frac{1}{f} \tag{3.17}$$

Thus the Gaussian window

$$g(t, \sigma) = \frac{1}{\sqrt{2\pi}\sigma} e^{-\frac{t^2}{2\sigma^2}} \tag{3.18}$$

with $\sigma = \frac{1}{f}$ becomes

$$g(t, \sigma) = \frac{f}{\sqrt{2\pi}\sigma} e^{-\frac{t^2 f^2}{2}} \tag{3.19}$$

and

$$G(\alpha, f) = e^{-\frac{2\pi^2\alpha^2}{f^2}} \tag{3.20}$$

Equation 3.20 is derived from the Fourier Transform pair,

$$e^{-at^2} \leftrightarrow \sqrt{\frac{\pi}{a}} e^{-\frac{\omega^2}{4a}} \tag{3.21}$$

which for a Gaussian function

$$g(t, \sigma) = \frac{1}{\sqrt{2\pi}\sigma} e^{-\frac{t^2}{2\sigma^2}} \tag{3.22}$$

becomes

$$\frac{1}{\sqrt{2\pi}\sigma} e^{-\frac{t^2}{2\sigma^2}} \leftrightarrow \frac{1}{\sqrt{2\pi}\sigma} \sqrt{\pi 2\sigma^2} e^{-\frac{\omega^2}{4} 2\sigma^2} \tag{3.23}$$
$$\leftrightarrow e^{-\frac{\omega^2\sigma^2}{2}} \tag{3.24}$$

The S-Transform can be defined as a CWT with a specific mother wavelet multiplied by a phase factor.

$$S(\tau, f) = e^{i2\pi ft} W(\tau, d) \tag{3.25}$$

where

$$W(\tau, d) = \int_{-\infty}^{\infty} h(t) w(t - \tau) dt \tag{3.26}$$

is the Wavelet Transform of a function $h(t)$ with a mother wavelet $w(t, f)$, defined as

$$w(t, f) = \frac{|f|}{\sqrt{2\pi}} e^{-\frac{t^2 f^2}{2}} e^{-i2\pi ft} \tag{3.27}$$

The S transform separates the mother wavelet into two parts,the slowly varying envelope (the Gaussian function) which localizes in time,and the oscillatory exponential kernel $e^{-2\pi ft}$ which selects the frequency being localized. It is the time localizing Gaussian that is translated while the oscillatory exponential kernel remains stationary. By not translating the oscillatory exponential kernel, the S-Transform localizes the real and the imaginary components of the spectrum independently, localizing the phase spectrum as well as the amplitude spectrum. This is referred to as absolutely referenced phase information. The ST produces a time frequency representation instead of the time scale representation developed by the WT. Figure 3.1 pictures the time frequency representation of the test time series described in Chapter 2. The time and frequency locations of the time series in the time frequency plane can be directly read out from the plot.

The S-transform is a method of spectral localization. It can be applied to fields that require the calculation of event initiation. It has found applications in many fields [6] including Geophysics [2][7] , Biomedical Engineering [8][9], Genomic Signal Processing, Power transformer protection [10][11][12].

3.3 Comparison of S Transform and CWT

In [13], Stockwell compares the S transform and the Continuous Wavelet transform. The major differences between the S transform and CWT are :

1. **Frequency Sampling** : The discrete Fourier transform has a very definite sampling of the frequencies, in order to be both complete and orthonormal. The discrete ST has the identical sampling of the frequency space. It also retains the sampling

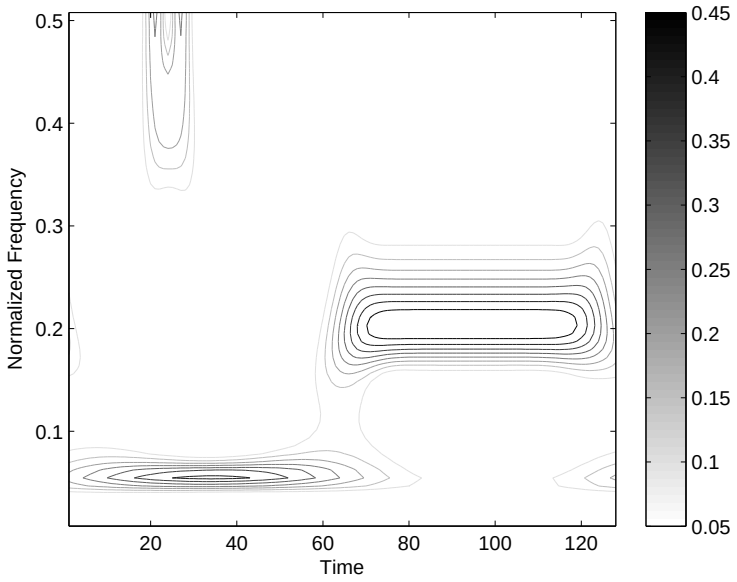

Figure 3.1: S Transform TFR of test time series

of the time series. On the other hand WT has a loosely defined scaling. It normally employs an octave scaling for frequencies,which results in an oversampled representation at the low frequencies and an under sampled representation at the higher frequencies.

2. **Direct Signal Extraction** : The amplitude, frequency and phase at any time instant can be directly measured from the S transform. A time domain signal can be extracted form the above measurements.

$$Signal(t) = A(t)cos(2 * pi * f(t) * t + \phi(t)) \tag{3.28}$$

where $A(t)$,$f(t)$ and $\phi(t)$ are the amplitude, frequency and phase at any time instant t.This direct extraction of a signal is due to the combination of absolutely referenced phase information and frequency invariant amplitude of the S-transform, and such direct extraction cannot be done with Wavelet methods.

3. **ST Phase** : The ST retains the absolute phase information, where as the phase information is lost in the WT. The absolutely referenced phase of the S-transform is in contrast to a wavelet approach, where the phase of the wavelet transform is relative to the center (in time) of the analyzing wavelet. Thus as the wavelet translates, the reference point of the phase translates. In ST, the sinusoidal component

of the basis function remains stationary, while the Gaussian envelope translates in time. Thus the reference point for the phase remains stationary.

4. **ST Amplitude** : The unit area localizing function (the Gaussian) preserves the amplitude response of the S-transform and ensures that the amplitude response of the ST is invariant to the frequency. In much the same way that the phase of the ST means the same as the phase of the Fourier transform, the amplitude of the ST means the same as the amplitude of the Fourier transform. On the other hand, WT diminishes the higher frequency components.

3.4 Generalized S Transform

McFadden et al. [14] and later Pinnegar and Mansinha [15] introduced a generalized S-transform which has a greater control over the window function. The generalized S transform is given by

$$S(\tau, f, \beta) = \int_{-\infty}^{\infty} h(t) w(\tau - t, f, \beta) e^{-j2\pi ft} dt \tag{3.29}$$

where w is the window function of the S transform and β denotes the set of parameters that determine the shape and property of the window function. τ is a parameter that controls the position of the Generalized window w on the time axis. For the Gaussian window w_{GS} [16], γ is the only parameter in β and it controls the width of the window

$$w(\tau - t, f, \gamma) = \frac{|f|}{\gamma\sqrt{2}\pi} exp\left[-\frac{f^2(\tau - t)^2}{2\gamma^2}\right] \tag{3.30}$$

If the generalized window w satisfies the following normalization criteria,

$$\int_{-\infty}^{\infty} w(\tau - t, f, \beta) d\tau = 1 \tag{3.31}$$

then

$$\int_{-\infty}^{\infty} S(\tau - t, f, \beta)d\tau = \int_{-\infty}^{\infty}\int_{-\infty}^{\infty} h(t)e^{-i2\pi ft}w(\tau - t, f, \beta)dtd\tau \tag{3.32}$$

$$= \int_{-\infty}^{\infty} h(t)e^{-i2\pi ft}\int_{-\infty}^{\infty} w(\tau - t, f, \beta)d\tau dt \tag{3.33}$$

$$= \int_{-\infty}^{\infty} h(t)e^{-i2\pi ft}dt \tag{3.34}$$

$$= H(f) \tag{3.35}$$

where $H(f)$ is the Fourier transform of the signal $h(t)$.

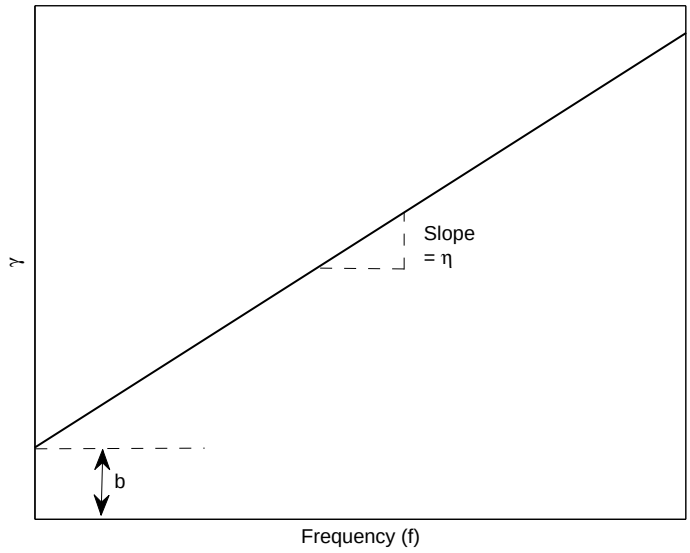

Figure 3.2: Scaling function γ

3.5 Modified S Transform

In the modified S transform, we are using a different scaling rule for the Gaussian window. The scaling function γ is made a linear function of frequency.

$$\gamma(f) = \eta f + b \tag{3.36}$$

where η is the slope and b is the intercept. The resolution in time and in frequency depends on both η and b. We have determined usable values of η and b by trial and error.

The modified S transform becomes

$$S(\tau, f, \eta, b) = \int_{-\infty}^{\infty} h(t) w(\tau - t, f, \eta, b) e^{-j2\pi ft} dt \tag{3.37}$$

where w denotes the window function of the modified S transform, denoted by

$$w(\tau - t, f, \eta, b) = \frac{|f|}{\sqrt{2}\pi(\eta f + b)} e^{-\frac{(\tau - t)^2 f^2}{2(\eta f + b)^2}} \tag{3.38}$$

Using (3.37) and (3.38),

$$S(\tau, f, \eta, b) = \int_{-\infty}^{\infty} h(t) \frac{|f|}{\sqrt{2}\pi(\eta f + b)} e^{-\frac{(\tau - t)^2 f^2}{2(\eta f + b)^2}} e^{-j2\pi ft} dt \tag{3.39}$$

The modified S transform also satisfies the normalization condition for S transform windows and hence is invertible.

$$\int_{-\infty}^{\infty} \frac{|f|}{\sqrt{2}\pi(\eta f + b)} e^{-\frac{(\tau - t)^2 f^2}{2(\eta f + b)^2}} d\tau = 1 \tag{3.40}$$

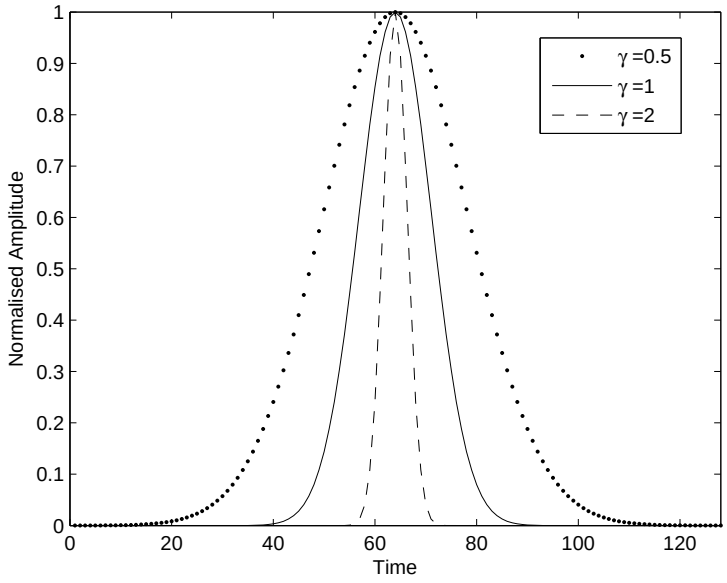

Figure 3.3: Variation of window width with γ for a particular frequency($25Hz$)

The parameter γ represents the number of periods of the Fourier sinusoid that can be contained within one standard deviation of the Gaussian window. The time resolution i.e. the event onset and offset time and frequency smearing is controlled by the factor

γ. If γ is too small the Gaussian window retains very few cycles of the sinusoid. Hence the frequency resolution degrades at low frequencies. If γ is too high the window retains more sinusoids within it and as a result the time resolution degrades at high frequencies. It indicates that the γ value should be varied with care for better energy distribution in the time-frequency plane.

Typical range of η is $0.25 - 0.5$ and b is $0.5 - 3$. The variation of width of window with γ for a particular frequency component (25 Hz) is illustrated in Fig. 3.3. The value of η and b need to be selected depending on the type and nature of the signal under consideration.

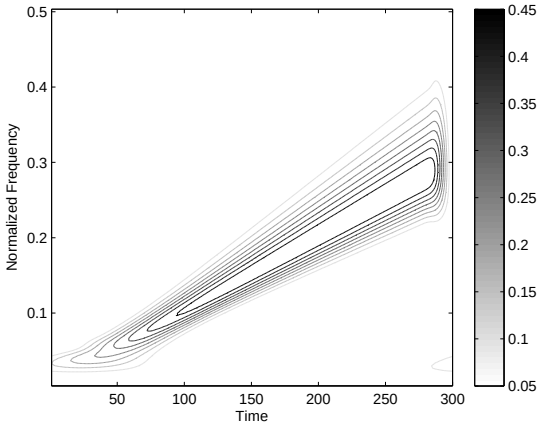

(a) Example 1 - TFR Using S Transform

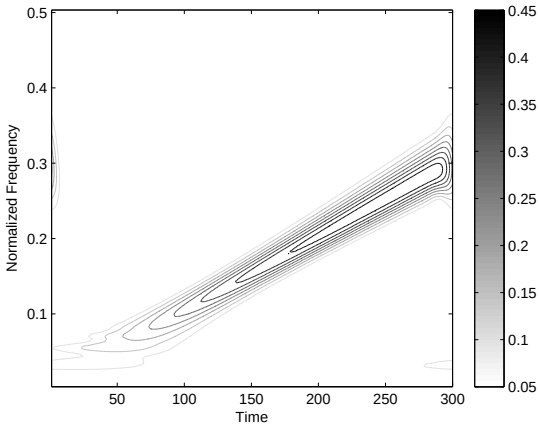

(b) Example 1 - TFR Using Modified S Transform

Figure 3.4: Example 1 - TFR Using S Transform and Modified S Transform

3.6 Simulation and Discussion

The time frequency resolution characteristics of the modified S transform is tested using a set of test signals.

3.6.1 Example 1

The first test signal is a linear chirp signal. The instantaneous frequency of a linear chirp signal varies linearly with time. The instantaneous frequency is given by

$$f_i(t) = f_0 + \kappa t \tag{3.41}$$

where

$$\kappa = (f_1 - f_0)/t_1 \tag{3.42}$$

κ ensures that the desired frequency breakpoint f_1 at time t_1 is maintained. f_1 and f_0 are two frequency points through which the signal traverses. For this example, the time t is made to vary from -1 to 1.99 with a sampling period of 0.01 . The test signal can be generated in MATLAB using the following commands.

$$t = -1 : 0.01 : 1.99;$$
$$h = chirp(t, 10, 1, 20);$$

Figure 3.4 shows the difference in time frequency resolution using S transform and modified S transform with $\eta = 0.25$ and $b = 1.9$.

3.6.2 Example 2

The second test signal that is a combination of a linear and a quadratic chirp signal. The frequency of the quadratic chirp increases quadratically. The linear chirp has a frequency characteristics, that decreases linearly with time. The instantaneous frequency of a quadratic chirp signal is given by

$$f_i(t) = f_0 + \kappa t^2 \tag{3.43}$$

where

$$\kappa = (f_1 - f_0)/t_1^2 \tag{3.44}$$

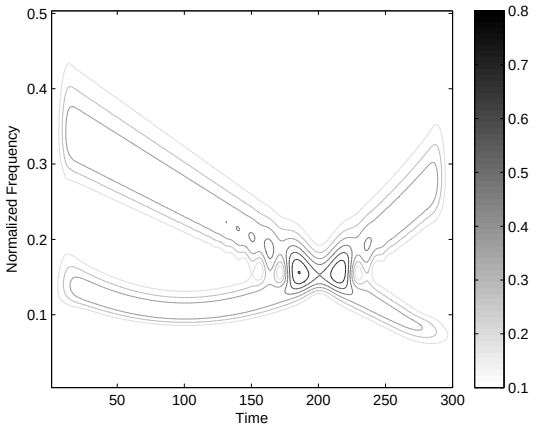

(a) Example 2 - TFR Using S Transform

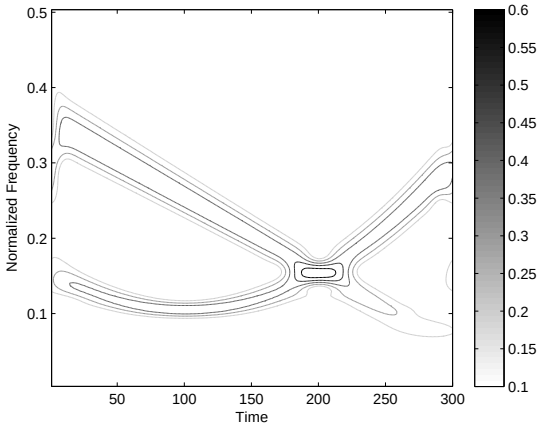

(b) Example 2 - TFR Using Modified S Transform

Figure 3.5: Example 2 - TFR Using S Transform and Modified S Transform

κ ensures that the desired frequency breakpoint f_1 at time t_1 is maintained. f_1 and f_0 are two frequency points through which the signal traverses. If $f_0 > f_1$, the chirp signal will have a convex frequency behavior and if $f_1 > f_0$, the signal will have a concave frequency pattern. The test signal can be generated in MATLAB using the following commands

$$t = -1 : 0.01 : 1.99;$$
$$h = chirp(t, 10, 1, 15, `quadratic') + chirp(t, 25, 1, 15);$$

Figure 3.5 depicts the TFR using original S transform and Modified S transform ($\eta = 0.25$ and $b = 1.9$). We can clearly see that the TFR using modified S transform has better

time frequency resolution compared to the original S transform.

3.7 Conclusion

The effective variation of the width of the Gaussian window can give better control over the energy concentration for the S-transform. This is achieved by introducing an additional parameter in the window which varies with frequency and thereby modulates the S-transform kernel efficiently with the progress of frequency. The proposed scheme is evaluated and compared with the standard S-transform by using a set of synthetic test signals. The comparison shows that the proposed method is superior to the standard one, providing a better time and frequency resolution. Hence the proposed S-transform can be widely used for analysis of all kinds of signal that need more time as well as frequency resolution.

4

Analysis of Business Cycles

4.1 Introduction

According to Parkin and Bade's text "Foundations of Economics" [17],a business cycle is the periodic but irregular up-and-down movements in economic activity, measured by fluctuations in real GDP and other macroeconomic variables. A business cycle is not a regular, predictable, or repeating phenomenon like the swing of the pendulum of a clock. Its timing is random and, to a large degrees, unpredictable. A business cycle is identified as a sequence of four phases:

- Contraction - A slowdown in the pace of economic activity
- Trough - The lower turning point of a business cycle, where a contraction turns into an expansion
- Expansion - A speedup in the pace of economic activity
- Peak - The upper turning of a business cycle

A severe contraction is called a recession. A particularly long-lasting and painful recession is known as a depression.

4.2 Causes of Business cycles

Just as there is no regularity in the timing of business cycles, there is no reason why cycles have to occur at all[18]. The prevailing view among economists is that there is a level of economic activity, often referred to as full employment, at which the economy could stay forever. Full employment refers to a level of production in which all the inputs to the production process are being used, but not so intensively that they wear out, break down, or insist on higher wages and more vacations. When the economy is at full employment, inflation tends to remain constant; only if output moves above or below normal does the rate of inflation systematically tend to rise or fall. If nothing disturbs the economy, the full-employment level of output, which naturally tends to grow as the population increases and new technologies are discovered, can be maintained forever. There is no reason why a time of full employment has to give way to either an inflationary boom or a recession.

Business cycles do occur, however, because disturbances to the economy of one sort or another push the economy above or below full employment. Inflationary booms can

be generated by surges in private or public spending. For example, if the government spends a lot to fight a war but does not raise taxes, the increased demand will cause not only an increase in the output of war matriel, but also an increase in the take-home pay of defense workers. The output of all the goods and services that these workers want to buy with their wages will also increase, and total production may surge above its normal, comfortable level. Similarly, a wave of optimism that causes consumers to spend more than usual and firms to build new factories may cause the economy to expand more rapidly than normal. Recessions or depressions can be caused by these same forces working in reverse. A substantial cut in government spending or a wave of pessimism among consumers and firms may cause the output of all types of goods to fall.

Another possible cause of recessions and booms is monetary policy. The Federal Reserve System strongly influences the size and growth rate of the money stock, and thus the level of interest rates in the economy. Interest rates, in turn, are a crucial determinant of how much firms and consumers want to spend. A firm faced with high interest rates may decide to postpone building a new factory because the cost of borrowing is so high. Conversely, a consumer may be lured into buying a new home if interest rates are low and mortgage payments are therefore more affordable. Thus, by raising or lowering interest rates, the Federal Reserve is able to generate recessions or booms. The following section discusses the Economic indicators [19], which are parameters that are directly or indirectly related to the economy and could possibly help in the analysis of business cycles.

4.3 Economic Indicators

An economic indicator is any economic statistic, such as the unemployment rate, GDP, or the inflation rate, which indicate how well the economy is doing and how well the economy is going to do in the future[18]. There are three major attributes each economic indicator has:

1. Relation to business cycles

   (a) **Procyclic** - A procyclic economic indicator is one that moves in the same direction as the economy. So if the economy is doing well, this number is usually increasing, whereas if we're in a recession this indicator is decreasing. The Gross Domestic Product (GDP) is an example of a procyclic economic indicator.

(b) **Countercyclic** - A countercyclic economic indicator is one that moves in the opposite direction as the economy. The unemployment rate gets larger as the economy gets worse so it is a countercyclic economic indicator.

(c) **Acyclic** - An acyclic economic indicator is one that has no relation to the health of the economy and is generally of little use.

2. Frequency of the Data

   In most countries GDP figures are released quarterly (every three months) while the unemployment rate is released monthly. Some economic indicators, such as the Dow Jones Index, are available immediately and change every minute.

3. Timing

   Economic Indicators can be leading, lagging, or coincident which indicates the timing of their changes relative to how the economy as a whole changes.

   (a) **Leading** - Leading economic indicators are indicators which change before the economy changes. Stock market returns are a leading indicator, as the stock market usually begins to decline before the economy declines and they improve before the economy begins to pull out of a recession. Leading economic indicators are the most important type for investors as they help predict what the economy will be like in the future.

   (b) **Lagged** - A lagged economic indicator is one that does not change direction until a few quarters after the economy does. The unemployment rate is a lagged economic indicator as unemployment tends to increase for 2 or 3 quarters after the economy starts to improve.

   (c) **Coincident** - A coincident economic indicator is one that simply moves at the same time the economy does. The Gross Domestic Product is a coincident indicator.

4.4 Types of business cycles

In [20], Schumpeter classifies business cycles based on their duration to five different classes.

- Seasonal cycles - within a year

- Kitchin cycles - 3 years
- Juglar cycles - 9-10 years
- Kuznets cycles - 15-20 years
- Kondratiev cycles - 48-60 years

He also defines a 'cycle' as a loop of four stages : boom-recession-depression-recovery. Starting from the mean, a boom is a rise which lasts until the peak is reached; a recession is the drop from the peak back to the mean; a depression is the slide from the mean down to the trough; a recovery is the rise from the trough back up to the mean. From the mean, we then move up into another boom and thus the beginning of another four-phase cycle. In a sense, any cycle of whatever duration can be described as going through these four phases.

4.4.1 Kondratiev cycles

Kondratiev or K-waves are regular, sinusoidal cycles in the modern world economy. Averaging fifty and ranging from approximately forty to sixty years in length, the cycles consist of alternating periods between high sectoral growth and periods of slower growth. Simon Kuznets,(1901-1985) classifies Kondratiev cycles or long waves into four major classes.

- **The Industrial Revolution (1787-1842)**- The industrial revolution cycle is the most famous Kondratiev wave. The boom began in about 1787 and turned into a recession at the beginning of the Napoleonic age in 1801 and, in 1814, deepened into a depression. The depression lasted until about 1827 after which there was a recovery until 1842. As is obvious, this Kondratiev rode on the development of textile, iron and other steam-powered industries.
- **The Bourgeois Kondratiev (1843-1897)**: After 1842, the boom reemerged and a new Kondratiev wave began, this one as a result of the development of road and rail networks in Northern Europe and America and the accompanying expansion in the coal and iron industries. The boom ended approximately in 1857 when it turned into a recession. The recession turned into a depression into 1870, which lasted until about 1885. The recovery began after that and lasted until 1897.

- **The Neo-Mercantilist Kondratiev (1898-1950)**: The boom began about 1898 with the expansion of electric power and the automobile industry and lasted until about 1911. The recession which followed turned into depression in about 1925 which lasted until around 1935.

- **The Fourth Kondratiev (1950- 2000)** : There has been much debate among econometricians on the dating the Fourth Wave - largely because of the confusions generated by the low fluctuation in price levels and the issue of Keynesian policies and hence this debate is yet to be resolved. Perhaps the most acceptable set of dates is that the boom began around 1950 and lasted until about 1974 wherein recession set in. In and around 1981 there was a depression followed by a recovery that lasted upto around 1992.

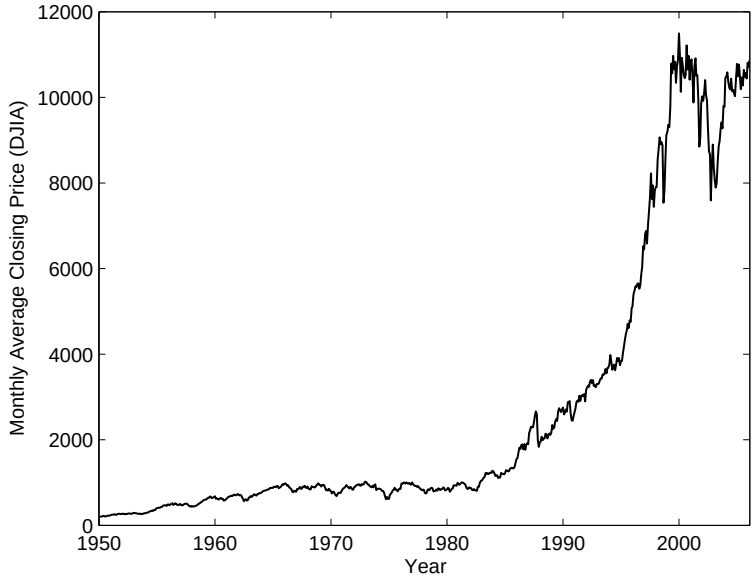

Figure 4.1: Monthly Average Closing Price - DJIA

All economic time series are generally non stationary in nature. This makes time frequency analysis, one of the most suitable methods for the analysis of econometric data. In the following section, the S transform discussed in Chapter 3 is applied to different economic indicators to study the cyclic behavior of business cycles.

4.5 Analysis and Discussion

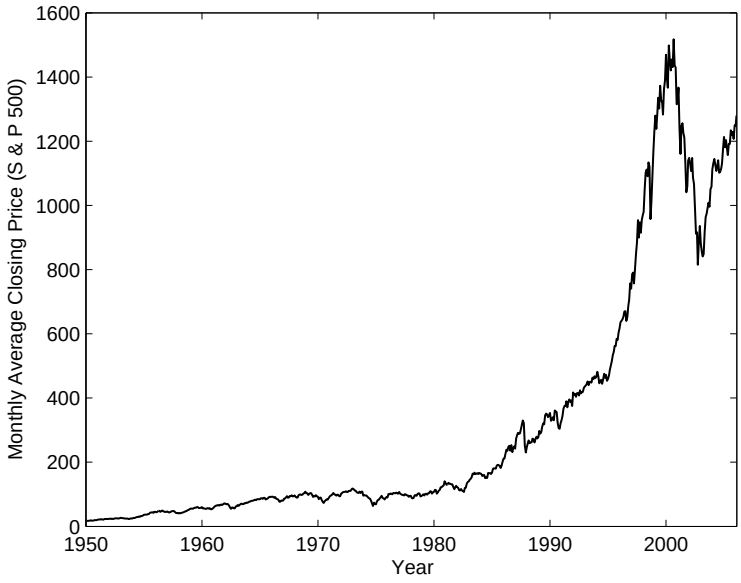

Figure 4.2: Monthly Average Closing Price - S&P 500

Since Second World War, the US economy has experienced several important institutional changes. These institutional changes have likely had important impact on the structure of the US economy. The US economy has also experienced several unprecedented shocks that may also have brought deep structural adjustment to the economy. The oil price shock during the early 70s, for example, could have resulted in a fundamental reorganization of the input-output structure in the economy, especially with regard to the energy-intensive industries.

As explained in section 4.3, stock market is a leading economic indicator(indicators that change before the economy changes). For the analysis of business cycles, two sets of stock market data from the Unites States are taken. One from the Dow Jones Industrial Average (DJIA), USA, and the other from the Standards & Poors 500 Index (S&P 500),USA. The time series data of all the stock indices (monthly data) were collected from January 1950 to January 2006. Thus there were 673 data patterns for both DJIA and S&P 500 index. Applying the S transform based time frequency analysis on the two independent stock indices in the United States, the following conclusions can be inferred on the business cycles.

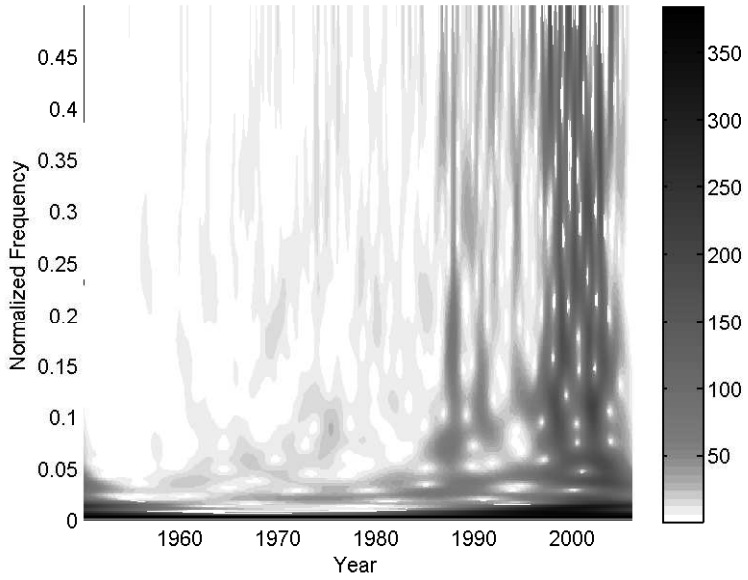

Figure 4.3: S Transform - DJIA

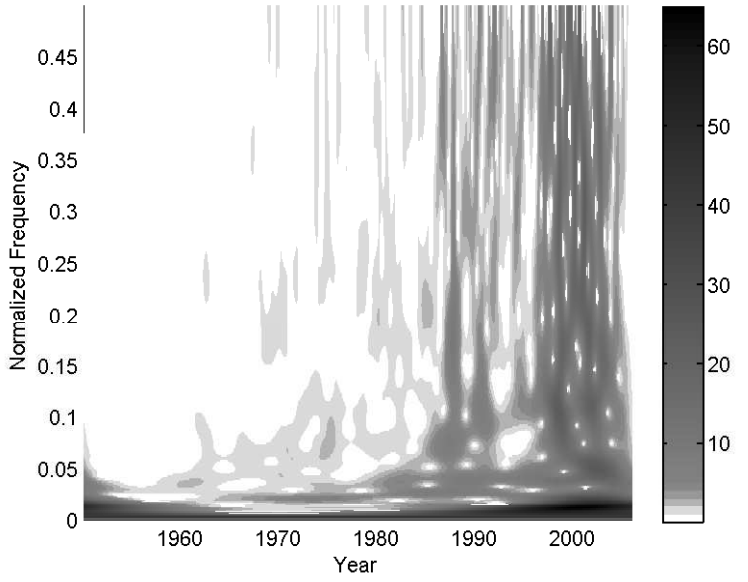

Figure 4.4: S Transform - SNP

1. A long cycle exists through out the time series. It reflects the slow pace of structural changes in the economy.

2. There have been three major short duration business cycles since 1960. The first

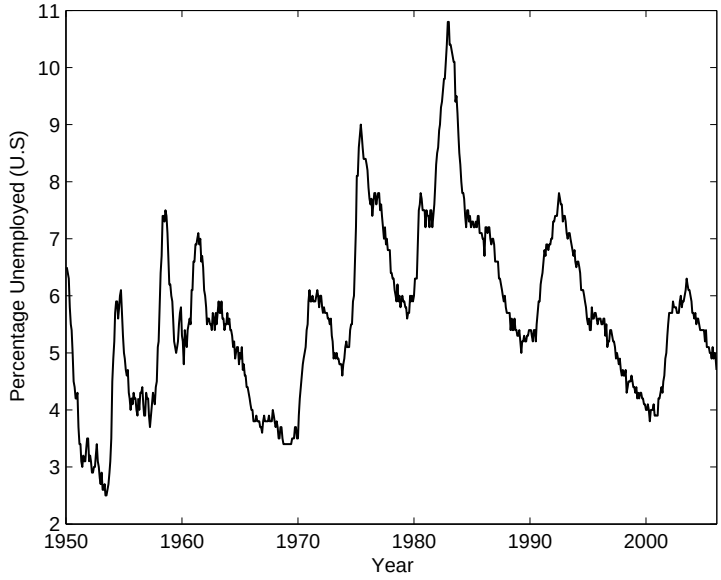

Figure 4.5: Percentage Unemployed (U.S)

occurred in 1961, triggered by a sharp external impulse during that year. The 1961 cycle has a frequency of 30 months per cycle and is short lived.

3. The second major cycle took place in 1973, apparently triggered by two impulses during 1972 and 1973, and was greatly intensified by another impulse near 1975 [21]. This business cycle lasted about 3-4 years and peaked at the frequency of about 70 months per cycle).

4. The third major cycle occurred during 1982-1984, apparently triggered by a shock in 1982. This cycle lasted about 3 years and peaked also at a frequency similar to the 1973 cycle.

5. There exists a short-lived business cycle in 1966 triggered by an external impulse.

According to International Monetary Fund (IMF) working paper on the evolution of business cycles [22] , the nature of world business cycles has changed over time due to 'globalization', which is often associated with rising trade and financial linkages. It is indeed the case that globalization has picked up momentum in recent decades. For example, the cumulative increase in the volume of world trade is almost three times larger than that of world output since 1960. More importantly, there has been a striking increase in the volume of international financial flows during the past two decades as

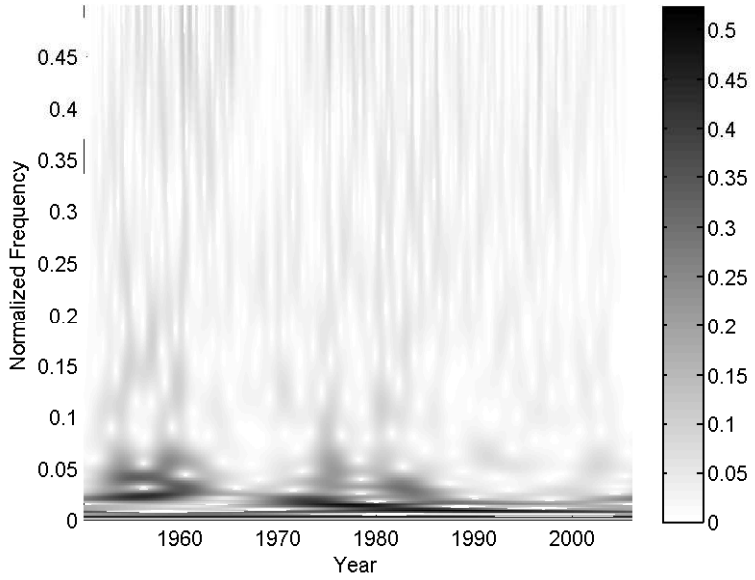

Figure 4.6: S Transform TFR - Unemployment

these flows have jumped from less than 5 percent to approximately 20 percent of GDP of industrialized countries. Recent empirical studies are also unable to provide a concrete explanation for the impact of stronger trade and financial linkages on the nature of business cycles.

Similar to the stock prices, percentage unemployed in a country is a direct indicator of the condition of an economy. In order to study the behavior of unemployment, a time frequency analysis was done on the United States Percentage Unemployed data. The data was collected from January 1950 to January 2006, the same period of study of the stock market time series. The unemployment rate time series (Figure 4.5) show a cyclic behavior, but the frequency of the cycle cannot be inferred directly from the time domain signal. Figure 4.6 depicts the time frequency representation of the unemployment rate time series using S transform. There exists a low frequency cycle at around 0.02 (normalized frequency).Time period of the unemployment cycle = 1/0.02 = 50 months,which turns out to be very close to the presidential tenure in the United States (4 years).

Oil price is an economic indicator which can directly affect the state of the world economy. The rise in oil price can lead to economic crisis. Figure 4.7 shows the oil price in US dollars/barrel from January 1950 to January 2006 (673 data samples). The time frequency analysis of oil price (Figure 4.8) reveals that there is repetitive cycle of around 0.1 (Normalized Frequency), which repeats itself in 1974,1981,1983,1986,1990-

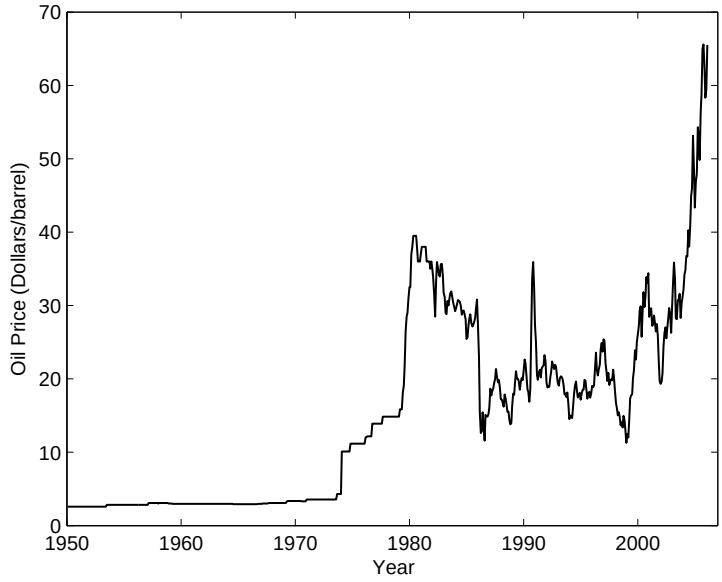

Figure 4.7: Oil Price (US Dollars/barrel)

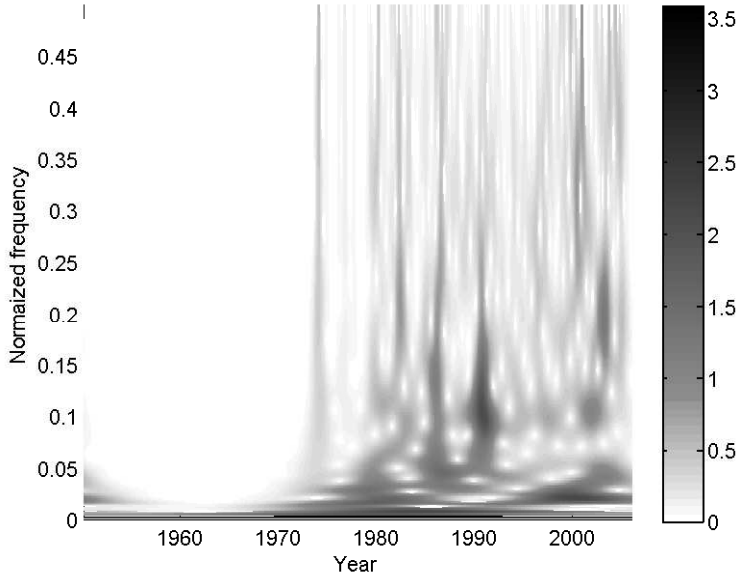

Figure 4.8: S Transform TFR - Oil Price

91 and 2001. The possible reason(s) for the 0.1 frequency cycle is pictured in Table 4.1,where the cycles are in close match with the oil price peaks observed by Walter Labys [23]. There also exists another low frequency component that exists almost through out the duration of study. The low frequency is around 50 months which is coinciding with both the unemployment cycle, which in turn almost matches with the US presidency cycle.

Table 4.1: Oil Price Peaks

Year	Possible Reason
1974	Arab oil production embargo
1979	Fall of the Shah of Iran
1981	Afghan War
1983	Afghan War
1986	Iran-Iraq War
1991	Gulf War
2001	Iraq-US War

4.6 Conclusion

The time frequency analysis of economic indicators have revealed the existence of business cycles of different durations in an econometric time series. The relation between unemployment, oil price and the economic situation of a country could be identified from the study. The analysis results can be combined with other economic indicators to forecast the behavior of global economy.

5

Time Frequency Filtering - An Alternate Approach

5.1 Introduction

Standard frequency domain filtering approaches have a fixed stop band and pass band for the entire time duration.Since most of the natural time series are non-stationary, there is a need for filters with variable pass bands and stop bands. Linear time-varying (LTV) filter is such type of a filter which have a dynamic cutoff frequency. i.e. The cutoff frequency varies with time. LTV filters have important applications including non-stationary statistical signal processing (signal detection and estimation, spectrum estimation, etc.) and communications over time-varying channels (interference excision, channel modeling, estimation, equalization, etc.). LTV filters are particularly useful for weighting, suppressing or separating non-stationary signal components[24].

The input output relation for a linear time varying filter, **H**, is given by

$$y(n) = \mathbf{H}.x(n) \tag{5.1}$$

where $x(n)$ is the filter input and $y(n)$ is the LTV filter output.

Time Frequency (TF) representations can be used to implement a LTV filter, when either $x(n)$, $y(n)$ or **H** is non-stationary. The need for a time varying filter can be explained using Figure 5.1. The figure represents the time frequency representation of a synthetic signal. The synthetic signal is composed of two time series. One is a noise component, which is represented by the black region of the TF representation. The grey region shows the signal component of the composite signal. A filter need to be designed to remove the noise component of the composite signal without affecting the signal component. The filter **H** should pass the signal components and should block the noise components. These type of signals cannot be filtered using a Fourier domain filter as the cutoff frequency is different at different time locations (i.e. varying with time). A possible solution is the time varying filter, whose cutoff frequency varies with time. The specification of the filter **H** can be expressed as a TF weighting function, $M(\tau, f)$, which is effectively '1' over the signal regions and is '0' for the noise regions.

The two different general approaches to designing a Linear Time Varying filters are -

1. **Explicit Design** - The LTV filter **H** is designed to closely match the weighing function,$M(\tau, f)$. The filtering is performed in the time domain using (5.1).

2. **Implicit Design** - The LTV filter **H** is designed implicitly during the filtering, which is an analysis-weighting-synthesis procedure. A linear TF representation of the input signal $x[n]$ is first calculated. The TF representation is multiplied by the

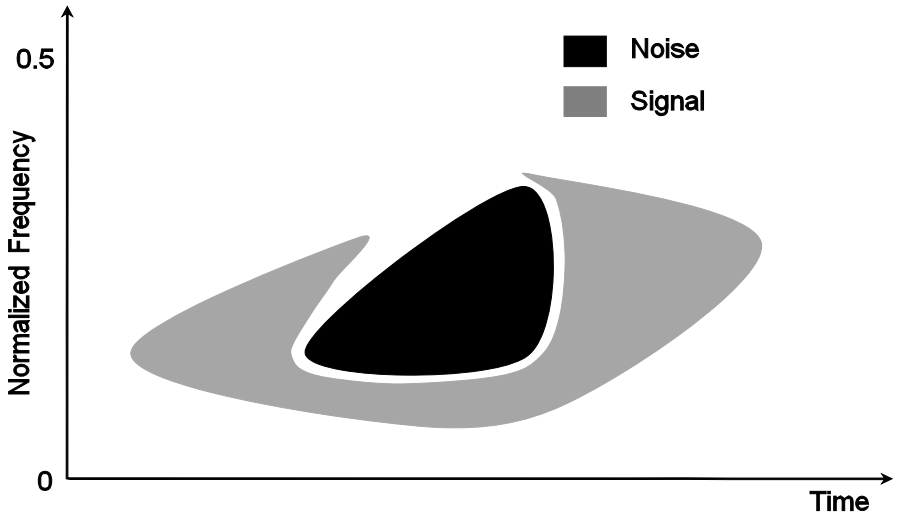

Figure 5.1: Need for LTV filters

TF weighing function $M(\tau, f)$. The resulting TF representation, is inverted to the time domain to recover the time domain filtered signal $y[n]$.

5.2 Literature Survey

Time Frequency filters are similar in concept to Fourier domain filters, except the addition of a second dimension to the filter. The TF filters converts the time domain signal to the time frequency distribution, followed by a selective excision of the stop band regions, and a re-transformation to the time domain using the corresponding inverse time frequency transform. In [25], Saleh and Subotic used Wigner Distribution (WD) and Short Time Fourier Transform (STFT) as the time frequency distribution. The WD gives good time frequency resolution, except that WD produces cross terms that are problematic in filtering. They also tried the TF filtering using STFT. STFT uses the same analyzing window for all the frequencies and hence have poor time frequency resolution.

In [26], Pinnegar used S transform as the time frequency distribution for TF filtering. The S transform, which is a modified STFT, gives good time frequency resolution compared to STFT. S Transform is a linear transform and hence has no cross term artifacts. The S transform of a signal $x[n]$ is given by

$$S[\tau, f] = \sum_{n=0}^{N-1} x[n]w[\tau - n, f]exp\left[\frac{-i2\pi fn}{N}\right] \tag{5.2}$$

where n and f are integer time and frequency indices. If T represents the sampling interval, nT gives the time in seconds and f/NT gives the frequency in Hz. The position of the S transform window w, is given by τ. The major difference between the STFT and the S transform is in the window function used. In STFT, a sliding window is used, whereas in S transform, a sliding window which scales in amplitude and width with frequency is used. A Gaussian window with an inverse relation between standard deviation σ and frequency f is normally used. The window function $w[\tau - n, f]$ is presented in 5.3.

$$w[\tau - n, f] = \frac{|f|}{N\sqrt{2\pi}} exp\left[\frac{f^2(\tau - n)^2}{2N^2}\right] \tag{5.3}$$

The width of the Gaussian part of w, as measured between the peak and the point having $1/\sqrt{e}$ the peak amplitude, is equal to $N/|f||$, the wavelength of the fth Fourier sinusoid. Thus, at any f , w always retains the same number of Fourier cycles[26]. The S transform is an invertible time frequency transform. The invertibility of the S transform depends on the window used in the analysis. For the S transform to be invertible, the window w should satisfy the normalization condition given by

$$\sum_{\tau=0}^{N-1} w\left[\tau - n, f\right] = 1 \tag{5.4}$$

When summed over all values of τ, the S transform (5.2) collapses to the Discrete Fourier Transform(DFT), X(f).

$$X[f] = \sum_{\tau=0}^{N-1} S[\tau, f] \tag{5.5}$$

An inverse DFT recovers the original time domain signal from the time frequency representation of S transform. The inverse S transform is given by

$$x[n] = \frac{1}{N} \sum_{f=-N/2}^{N/2-1} \sum_{\tau=0}^{N-1} S[\tau, f] exp\left[\frac{i2\pi ft}{N}\right] \tag{5.6}$$

Pinneger [26] introduced a 'boxcar' type filter which sets part of an S transform matrix equal to zero and keep all other values intact. The time frequency filter was tapered in the frequency direction to reduce artifacts due to sharp filters. These type of 'regular shaped' pass bands and stop bands are not practical when the pass band and stop band are very close together in the time frequency plane and when they are of 'irregular' shapes as in Figure 5.1. Another drawback of Pinneger's time frequency filter is that it cannot

remove background noise (Additive white Gaussian (AWG) Noise) , if any, present in the signal. The AWG noise in the time domain is usually spread across the complete time frequency plane, including the pass band. The filter in [26][27] can remove the AWG noise in the stop band as the complete signal in the stop band is removed. But it is not the case with the pass band. The AWG noise in the pass band of the filter remains in the filtered signal and hence is difficult to remove. The above mentioned two problems can be solved to a great extend using the following filtering approach.

5.3 The Proposed Filtering Approach

This novel filtering process is performed in two stages. In the first phase, the background noise is removed and then in the second stage the time limited and band limited noise components of the time series is removed. The filtering process kicks off with a time frequency representation of a time series using the modified S transform developed in Chapter 2. The modified S transform is used instead of the normal S transform as it gives better energy concentration than the original S transform.

5.3.1 Background Noise Removal

A low order 'best fit' surface is first developed by least square fitting of the $|S(\tau, f)|$. This surface acts as a reference for removing background noise. The difference between the S transform plane and the best fit quadratic surface is derived to form an intermediate surface. All data on the intermediate surface, which are less than three standard deviations of the Fourier transform are considered as part of the background noise spectrum and are removed from the S transform plane. For time series with very high signal amplitude compared to the background noise, a two stage fitting process is executed. An initial surface fitting is used to remove the highly prominent signal components from the time frequency plane. Another surface is fitted on the new time frequency plane obtained, which represents the true nature of the background noise, and is used as the reference surface for excision of background noise.

5.3.2 Localised Noise Filtering

The S transform plane obtained after background noise removal can be used as a foundation for filtering out localized unwanted signal elements. The ST plane is converted to a gray scale image, and the edges of the image are determined using a 'Laplacian for

Gaussian' edge detection technique. The Laplacian is a 2-D isotropic measure of the 2^{nd} spatial derivative of an image. The Laplacian of an image highlights regions of rapid intensity change. The Laplacian is applied to the image after smoothing the image with a spatial Gaussian filter in order to reduce its sensitivity to noise. If $I(x, y)$ denote the pixel intensity values of an image, the Laplacian, $L(x, y)$ can be calculated as:

$$L(x, y) = \frac{\partial^2 I}{\partial x^2} + \frac{\partial^2 I}{\partial y^2} \tag{5.7}$$

This operation produces an image that shows the edges of the signal and noise area as closed loops. The signal signatures which needed to be retained are 'whiteouted' using image filling techniques. Morphological dilation [28] is applied on the image to slightly 'grow' the signal regions in all directions on the image. The growth is intentionally made more prominent in the frequency direction of the S transform plane to reduce the artifacts of boxcar type filtering. The image after dilation forms a filter mask which is essentially the weighing function $M(\tau, f)$ described in Section 5.1. The product of the S transform surface and the filter mask removes the noise signatures. An Inverse S transform of the newly obtained S transform plane using (5.6) gives the filtered signal.

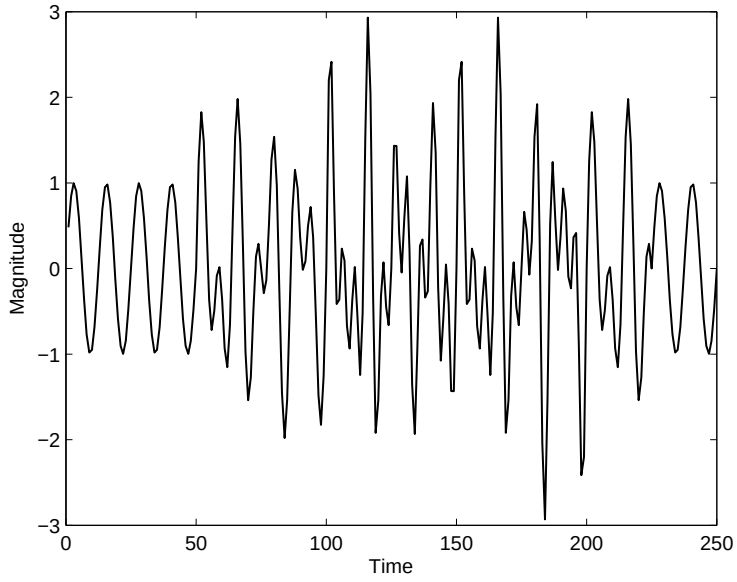

Figure 5.2: Example 1 - Input Signal

5.4 Simulation and Discussions

The performance of the filtering approach was tested using two different types of examples.

5.4.1 Example 1

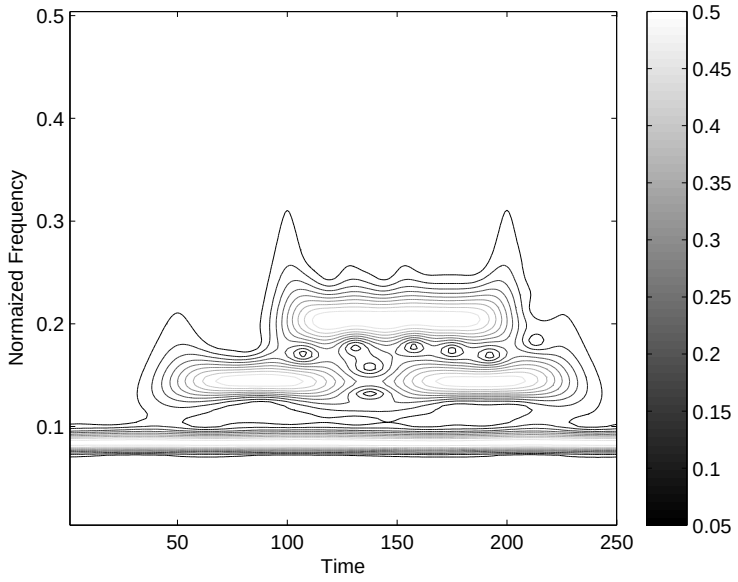

Figure 5.3: Example 1 - S Transform of the input signal

Figure 5.2 shows the first time series that was taken for the performance evaluation. The time series consists of four sets of sinusoidals at three different frequencies. The first sinusoidal is a 20Hz sinusoidal signal, which extends across the full length of the time series. The second signal is a 35Hz signal, which extends from samples 50 to 125 and from 150 to 225. The fourth set consists of a 50Hz sinusoidal signal which is time limited from 100 to 200 samples.

Figure 5.3 depicts the S transform contour plot of the test signal using the modified S transform with the parameters $\eta = 0.25$ and $b = 1.9$. The change in the S transform contour with the addition of Additive White Gaussian Noise (AWGN)can be clearly seen in Figure 5.4, which is the S transform contour of the test signal with a signal to noise ratio (SNR) of 10dB. A single stage quadratic surface (Figure 5.6) fitting was used for the first example to remove background noise. The 35Hz signal from samples 150 to

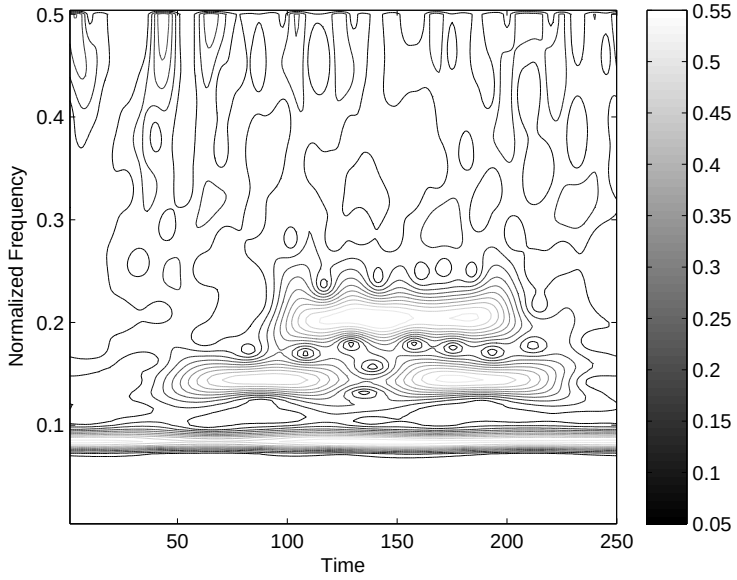

Figure 5.4: Example 1 - S transform of the input signal (SNR=10dB)

225 is considered here as an inband noise (i.e: 35Hz sinusoidal is part of the pass band from samples 50 to 125 and is part of the stop band from samples 150 to 225. The same frequency is present in the pass band and stop band).

Figure 5.5: Example 1 - Weighing Function

Using the image based techniques described in Section 5.3.2, a weighing function as shown in Figure 5.5 is obtained and is multiplies with the S transform surface to remove the inband noise. Figure 5.7 shows the desired filter output time series and the actual filter output time series. The filtering efficiency was quantitatively measured using the mean squared error (MSE).

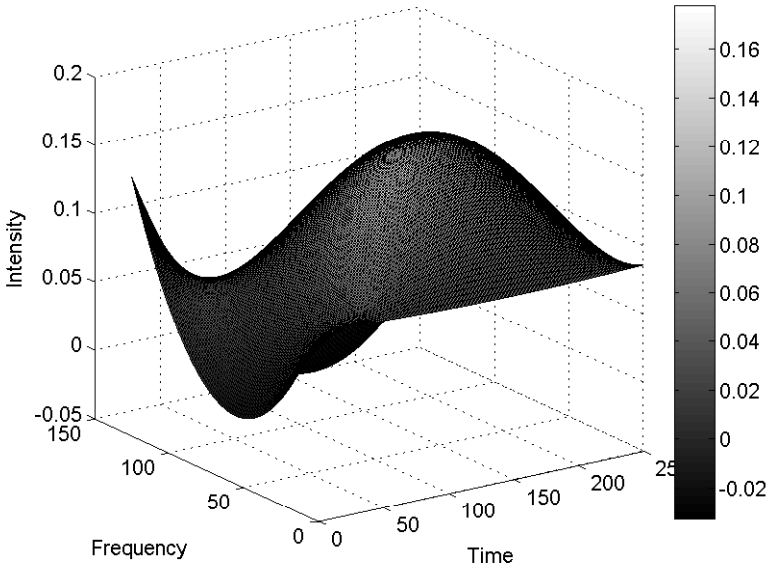

Figure 5.6: Example 1 - Noise Base

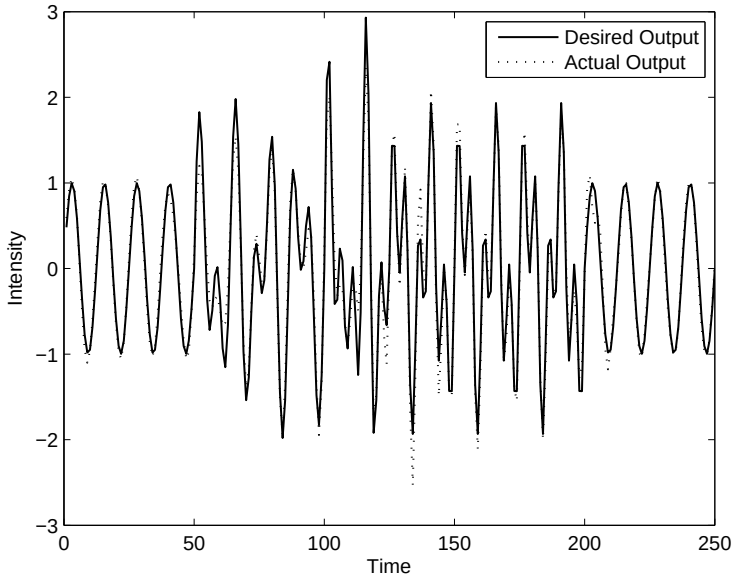

Figure 5.7: Example 1 - Filter Output

$$MSE = \frac{\sum_N \left[x(n) - \widetilde{x}(n)\right]^2}{N} \tag{5.8}$$

where $x(n)$ is the original time series, $\widetilde{x}(n)$ is the filtered time series and N is the length

of the time series. Table 5.1 shows the MSE for different values of SNR for the first example.

Table 5.1: Error Analysis : Example 1

SNR (dB)	MSE
10	0.0400
20	0.0293
30	0.0286
40	0.0277

5.4.2 Example 2

The second test series (Figure 5.8) contains two quadratic chirp signals: one is a time localized chirp and the other one is present across the full length of the time series. The time series is corrupted by AWGN.

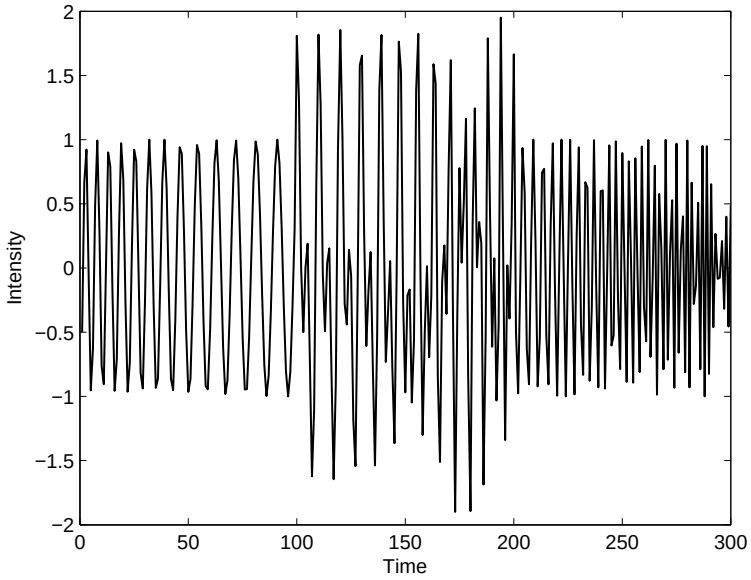

Figure 5.8: Example 2 - Input Signal

Figure 5.9 shows the TFR of the original time series , using the modified S transform

with the parameters $\eta = 0.25$ and $b = 1.9$. Figure 5.10 depicts the TFR of the test series corrupted with AWGN at an SNR of 10dB. On the TFR there appears a low magnitude background t-f spectrum (AWGN), with visible high magnitude spectral t-f components, which are the two chirp waveforms.

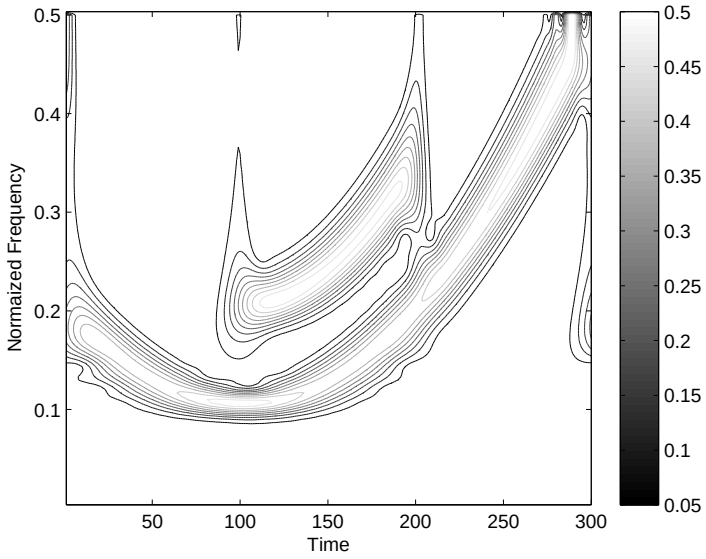

Figure 5.9: Example 2 - TFR using modified S transform

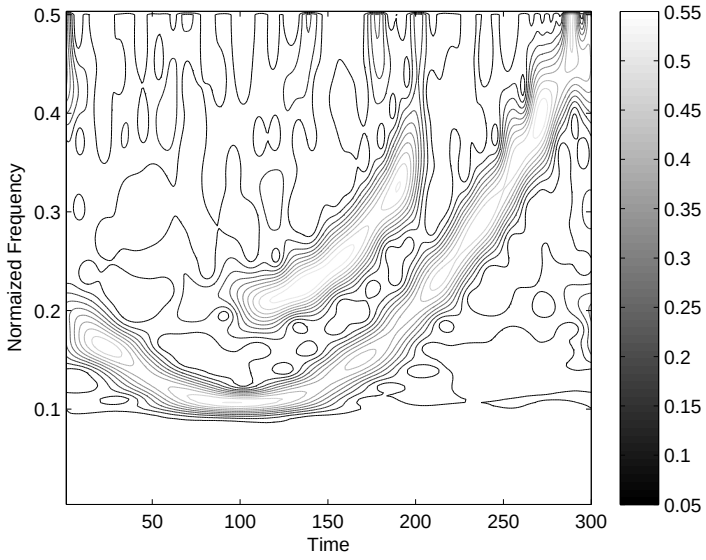

Figure 5.10: Example 2 - TFR of noisy signal using modified S transform

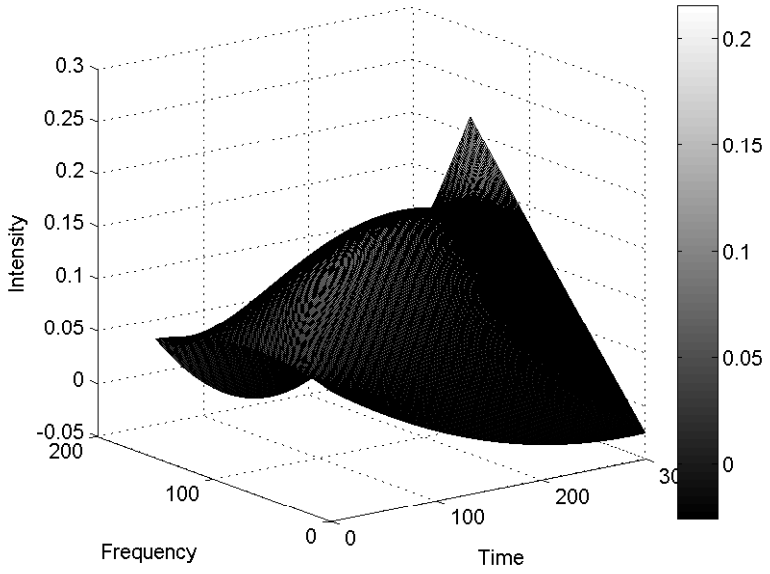

Figure 5.11: Example 2 - Reference surface for filtering out background noise

Since the test series has different amplitudes at different regions of time, a two stage curve fitting technique is employed. In the first stage fitting a quadratic 'best fit' surface is fitted to $|S(\tau, f)|$, the absolute value of the S transform matrix. This surface is used as a reference surface to remove the high amplitude signal components.

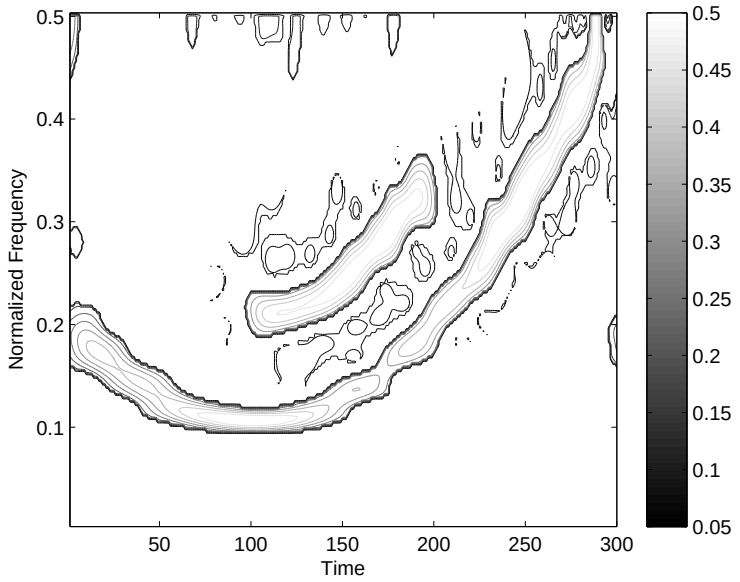

Figure 5.12: Example 2 - TFR after single surface fitting

The S transform matrix after removing the higher amplitude components is again fitted by a second quadratic surface, which acts as the ultimate reference surface for background noise removal as in Section 5.3.2. Figure 5.12 and Figure 5.13 shows the TF plane obtained after single stage and two stage surface fitting respectively. The background noise removal after dual stage fitting removes the background noise to a greater extend compared to single stage processing.

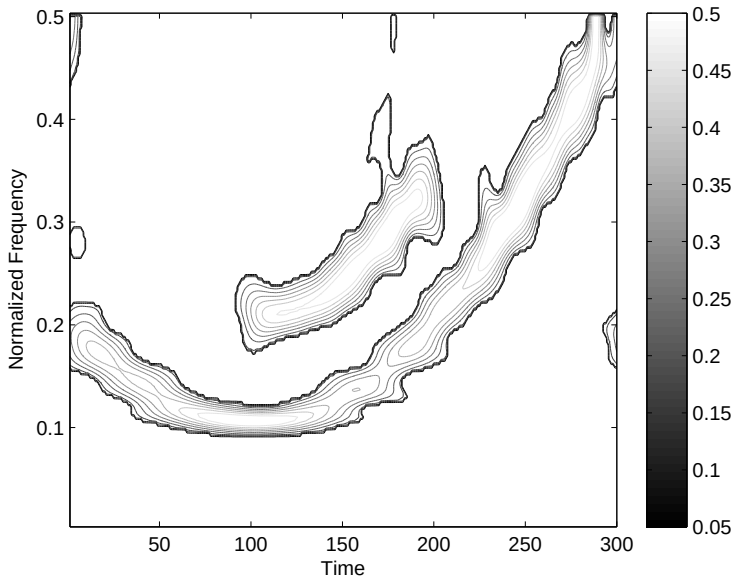

Figure 5.13: Example 2 - TFR after double surface fitting

The time frequency plane after background noise excision, is converted to an image and using the procedure explained in Section 5.3.2, a time frequency weighing plane is developed. The product of the S transform surface and the filter mask removes the noise signatures. An Inverse S transform of the newly obtained S transform plane using (5.6) gives the filtered signal. The results of this two stage filtration are checked with the S transform of the filtered signal (Figure 5.14). From the TFR, it is clear that the background noise as well as the time limited and band limited noise that were present in the test signal have been successfully removed and no extra signal components have been introduced.

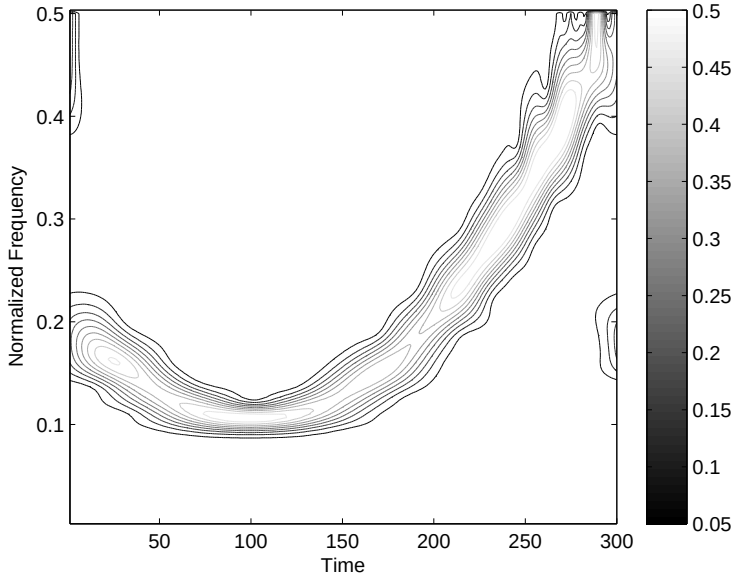

Figure 5.14: Example 2 - TFR of filtered signal

A second check is through the Mean Square Error (MSE) with the difference of the original and the filtered time series (Table 5.2).

Table 5.2: Error Analysis : Example 2

SNR (dB)	MSE
10	0.0203
20	0.0071
30	0.0063
40	0.0059

5.5 Conclusion

This chapter successfully demonstrated a new filtering scheme to remove background noise and localized noise from noisy time series. More work needs to be done to make this method operate for highly noisy signals.

6

Application to Geophysics

6.1 Introduction

Geophysics is the study of the Earth's subsurface and motions on its surface by the quantitative observation of its physical properties. Geophysical data are used to observe tectonic plate motions, study the internal structure of the Earth, supplement data provided by geologic maps, and to nondestructively observe shallow deposits. Geodesy is a field of geophysics, which is scientific discipline that deals with the measurement and representation of the Earth in a three-dimensional time-varying space. Points on the Earth's surface change their location due to a variety of mechanisms:

- Plate tectonics : It describes the large scale motions of Earth's lithosphere. The lithosphere is broken up into what are called tectonic plates. In the case of Earth, there are eight major and many minor plates. The lithospheric plates ride on the asthenosphere. These plates move in relation to one another at one of three types of plate boundaries: convergent, divergent or transform boundaries. Earthquakes, volcanic activity, mountain-building, and oceanic trench formation occur along plate boundaries.
- Periodic effects due to Earth tides
- Postglacial land uplift : It is rise of land masses that were depressed by the huge weight of ice sheets during the last glacial period.

Every motion estimation problem requires a reference point. A reference point on Earth cannot be used to calculate the relative motion of a point on the surface on the Earth. A possible solution is a reference point in space. The Global positioning satellites comes as a handy solution in determining the relative motion of a point on the surface of Earth.

6.2 Basic Concept of GPS

The Global Positioning System (GPS) is a global navigation satellite system (GNSS) developed by the United States Department of Defence and managed by the United States Air Force 50^{th} Space Wing. It uses a constellation of between 24 and 32 medium Earth orbit satellites that transmit precise radiowave signals, which allow GPS receivers to determine their current location, the time, and their velocity [29].

A GPS receiver calculates its position by precisely timing the signals sent by the GPS satellites high above the Earth. Each satellite continually transmits messages containing the time the message was sent, precise orbital information , and the general system health and rough orbits of all GPS satellites. The receiver measures the transit time of each message and computes the distance to each satellite. Geometric trilateration (A method for determining the intersections of three sphere surfaces given the centers and radii of the three spheres) is used to combine these distances with the location of the satellites to determine the receiver's location. The position is obtained as a latitude, longitude and elevation [30].

Three satellites are are enough to calculate the position. However a very small clock error multiplied by the very large speed of light (the speed at which satellite signals propagate) results in a large positional error. The receiver uses a fourth satellite to solve for x,y, z, and t which is used to correct the receiver's clock.

The GPS system consists of three segments [31]:

- Space segment
- Control segment
- User segment

All these parts operate together to provide accurate three-dimensional positioning, timing and velocity data to users worldwide.

6.2.1 Space segment

The GPS system constellation has 24 satellites in six 55^o orbital planes, with four satellites in each plane, with room for spares. The orbit period of each satellite is approximately 12 hours at an altitude of 20,183 kilometers. With this constellation, a user receiver has at least six satellites in view from any point on earth.

6.2.2 Control segment

The GPS control segment consists of a master control station,base stations and data up-loading stations in locations round the globe. Other configurations are possible for other satellite navigation systems. The base stations track and monitor the satellites via their broadcast signals. These signals are passed to the master control station where

orbital parameters and timing corrections are computed. The resulting corrections are transmitted back to the satellites via the data up-loading stations.

6.2.3 User Segment

An user segment consists of an equipment which track and receive the satellite signals. User segment must be capable of simultaneously processing the signals from a minimum of four satellites to obtain accurate position, velocity and timing measurements.

6.3 The Structure of the GPS signal

The principle of position determination by GPS and the accuracy of the positions strongly depend on the nature of the signals. GPS satellites transmit two low power radio signals, designated L1 and L2 [31]. Civilian GPS uses the L1 frequency of 1575.42 MHz in the UHF band. The signals travel by line of sight, meaning they will pass through clouds, glass and plastic but will not go through most solid objects such as buildings and mountains. A GPS signal contains three different bits of information a pseudorandom code, ephemeris data and almanac data. The pseudorandom code is simply an I.D. code that identifies which satellite is transmitting information. Ephemeris data, which is constantly transmitted by each satellite, contains important information about the status of the satellite (healthy or unhealthy), current date and time. This part of the signal is essential for determining a position. The almanac data tells the GPS receiver where each GPS satellite should be at any time throughout the day. Each satellite transmits almanac data showing the orbital information for that satellite and for every other satellite in the system.

6.3.1 Modulation of the carrier signals

C/A and P-Code

The carrier phases are modulated by three different binary codes: first there is the C/A code (coarse acquisition). This code is a 1023 'chip' long code, being transmitted with a frequency of 1.023 MHz. A 'chip' in the same as a 'bit', and is described by the numbers 'one' or 'zero'. The name 'chip' is used instead of 'bit' because no information is carried by the signal. By this code the carrier signals are modulated and the bandwidth of the man frequency band is spread from 2 MHz to 20 MHz (spread spectrum). Thus the

interference liability is reduced. The C/A code is a pseudo random code (PRN) which looks like a random code but is clearly defined for each satellite. It is repeated every 1023 bits or every millisecond. Therefore each second 1023000 chips are generated. Taking into account the speed of light the length of one chip can be calculated to be 300 m.

Pseudo Random Numbers (PRNs)

The satellites are identified by the receiver by means of PRN-numbers. Real GPS satellites are numbered from $1 - 32$. These PRN-numbers of the satellites appear on the satellite view screens of many GPS receivers. For simplification of the satellite network 32 different PRN-numbers are available, although only 24 satellites were necessary. The mentioned PRN-codes are only pseudo random. If the codes were actually random, 2^{1023} possibilities would exist. Of these many codes only few are suitable for the auto correlation or cross correlation which is necessary for the measurement of the signal propagation time. The 37 suitable codes are referred to as GOLD-codes. For these GOLD-codes the correlation among each other is particularly weak, making an unequivocal identification possible.

The C/A code is the base for all civil GPS receivers. The P code (precise) modulates the L1 as well as the L2 carrier frequency and is a very long 10.23 MHz pseudo random code. The code would be 266 days long, but only 7 days are used.For protection against interfering signals transmitted by an possible enemy, the P-code can be transmitted encrypted. During this anti-spoofing (AS) mode the P-code is encrypted in a Y-code. The encrypted code needs a special AS-module for each receiving channel and is only accessible for authorized personnel in possession of a special key. The P-code and Y-code are the base for the precise (military) position determination.

6.4 Errors in GPS

6.4.1 Satellite Geometry

Satellite geometry describes the position of the satellites to each other from the view of the receiver. If a receiver sees 4 satellites and all are arranged for example in the north-west, this leads to a 'bad' geometry. In the worst case, no position determination is possible at all, when all distance determinations point to the same direction. Even if a position is determined, the error of the positions may be up to 100150m. If, on the

other hand, the 4 satellites are well distributed over the whole firmament the determined position will be much more accurate.

6.4.2 Satellite Orbits

Although the satellites are positioned in very precise orbits, slight shifts of the orbits are possible due to gravitation forces. Sun and moon have a weak influence on the orbits. The orbit data are controlled and corrected regularly and are sent to the receivers in the package of ephemeris data. Therefore the influence on the correctness of the position determination is rather low, the resulting error being not more than 2m.

6.4.3 Multipath Effect

The multipath effect is caused by reflection of satellite signals on objects. For GPS signals this effect mainly appears in the neighborhood of large buildings or other elevations. The reflected signal takes more time to reach the receiver than the direct signal. The resulting error typically lies in the range of a few meters.

6.4.4 Atmospheric effects

Another source of inaccuracy is the reduced speed of propagation in the troposphere and ionosphere. While radio signals travel with the velocity of light in the outer space, their propagation in the ionosphere and troposphere is slower. In the ionosphere ($80400km$ above Earth's surface) a large number of electrons and positive charged ions are formed by the ionizing force of the sun. The electrons and ions are concentrated in four conductive layers in the ionosphere (D, E, F1, and F2 layer). These layers refract the electromagnetic waves from the satellites, resulting in an elongated runtime of the signals. These errors are mostly corrected by the receiver by calculations.

Electromagnetic waves are slowed down inversely proportional to the square of their frequency while passing the ionosphere. This means that electromagnetic waves with lower frequencies are slowed down more than electromagnetic waves with higher frequencies. If the signals of higher and lower frequencies which reach a receiver are analyzed with regard to their differing time of arrival, the ionospheric runtime elongation can be calculated. Military GPS receivers use the signals of different known frequencies which are influenced in different ways by the ionosphere and are able to eliminate another inaccuracy by calculation.

The tropospheric effect is a further factor elongating the runtime of electromagnetic waves by refraction. The reasons for the refraction are different concentrations of water vapour in the troposphere, caused by different weather conditions. The error caused that way is smaller than the ionospheric error, but can not be eliminated by calculation. It can only be approximated by a general calculation model.

6.4.5 Relativistic effects

The time is a relevant factor in GPS navigation and must be accurate to $20-30$ nanoseconds to ensure the necessary accuracy. Therefore the fast movement of the satellites themselves (nearly 12000 km/h) must be considered. According to the theory of relativity , time runs slower during very fast movements. For satellites moving with a speed of 3874 m/s, clocks run slower when viewed from earth. This relativistic time dilation leads to an inaccuracy of time of approximately 7.2 microseconds per day .

The theory of relativity also says that time moves the slower the stronger the field of gravitation is. For an observer on the earth surface the clock on board of a satellite is running faster (as the satellite in 20000 km height is exposed to a much weaker field of gravitation than the observer). And this second effect is six times stronger than the time dilation explained above. Altogether, the clocks of the satellites seem to run a little faster. The shift of time to the observer on earth would be about 38 milliseconds per day and would make up for an total error of approximately 10 km per day. In order that those error do not have to be corrected constantly, the clocks of the satellites were set to 10.229999995453 MHz instead of 10.23 MHz but they are operated as if they had 10.23 MHz. By this trick the relativistic effects are compensated once and for all.

Another relativistic effect is the Sagnac-Effect and is caused by the movement of the observer on the earth surface, who also moves with a velocity of up to $500m/s$ (at the equator) due to the rotation of the globe. The influence of this effect is very small and complicate to calculate as it depends on the directions of the movement. Therefore it is only considered in special cases.

6.5 Literature Survey

GPS signals have been used by geophysicists to study the post seismic deformation following an Earthquake. Post seismic deformation or deep earthquakes are small disturbances that occur after a major Earthquake. The post seismic deformation information is hid-

den deep inside the GPS signals due to the high amplitude seasonal and plate tectonic signals. In [32], K. F. Tiampo et. al studied the post seismic deformation following the Northridge Earth quake using Localized Hartley Transform Filter. Similar study have been done for many Earthquakes around the globe [33],[34],[35].

6.5.1 Glacial Isostatic Adjustment (GIA)

Glacial Isostatic Adjustment (Post-glacial rebound) is the rise of land masses that were depressed by the huge weight of ice sheets during the last glacial period, through a process known as isostatic depression [36]. It is sometimes called continental rebound, isostatic rebound, isostatic adjustment or post-ice-age isostatic recovery. It affects northern Europe , Canada, and the Great Lakes of Canada and the United States. For example, during the last glaciation which lasted roughly from 100,000 yr to 8,000 yr BP (before present), wide areas of North America and Scandinavia where covered by ice sheets extending over thousands of km and having thicknesses of up to 4 km. These loads depressed the earth's surface vertically down by hundreds of meters. After these ice sheets had molten away, the earth rebounded, but because the earth's mantle reacts like a highly viscous fluid this occurs rather slowly. These glacial loads are quite substantial.

Researchers have used the changes in the global tide height to measure Post glacial rebound[37]. Mazotti [38] and Johansson [39] used the GPS measurements to study the rebound effect. In this chapter we have used the GPS measurements from Eastern Canada to study the Post Glacial rebound in those regions.

6.6 Region of Study

A subset of the Canadian Base Network (CBN), consisting of thirty-nine GPS stations located throughout the region of seismicity of the lower Saint Lawrence valley, and stretches south through New England, east into southern Ontario, and north was taken for the analysis . The time period for this analysis begins in June of 2001 and finishes in June of 2006.

While the area of study is currently in an intra-plate tectonic setting, it is the historic location of several major tectonic events.Ice advanced over the Saint Lawrence valley during the late Pleistocene, as far east as the Maritime Provinces and south into New England. The weight of this ice depressed the lithosphere and the resulting viscoelastic flow in the mantle caused a peripheral bulge. Between 10k and 20k, the ice sheets

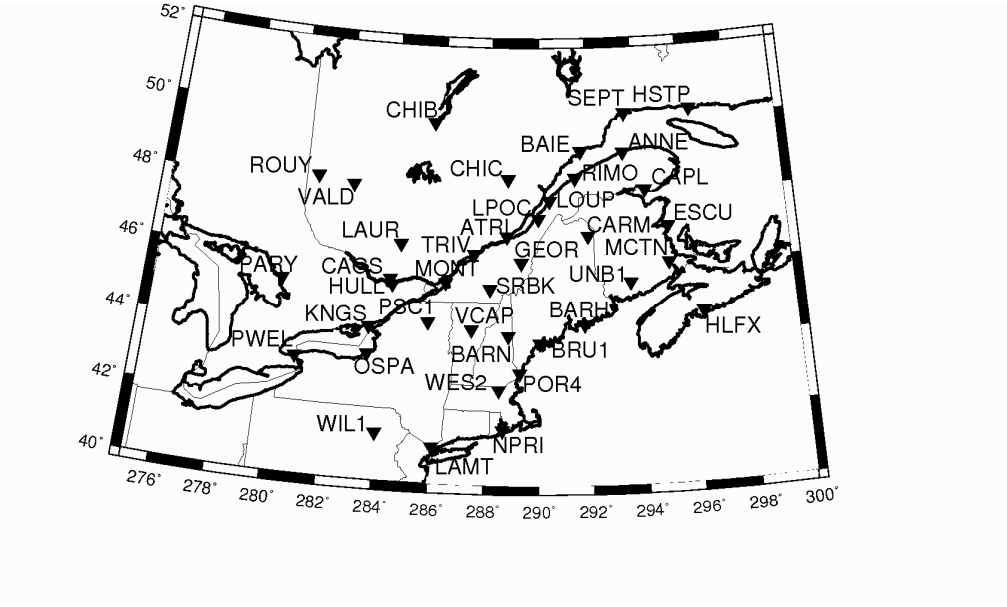

Figure 6.1: GPS Stations

began their retreat and the lithosphere began to rebound upward to regain isostatic equilibrium while the peripheral bulge began to migrate inward toward the centre of uplift as it gradually dissipated. This phenomenon is called Glacial Isostatic Adjustment(GIA) [explained in Section 6.5.1] and it is ongoing today. Uplift rates approach $10mm/yr$ or more at Hudson Bay and decrease with distance southward. Current GIA models forecast that the hinge line between uplift to the north and subsidence to the south lies somewhere near the Saint Lawrence valley in eastern Canada.

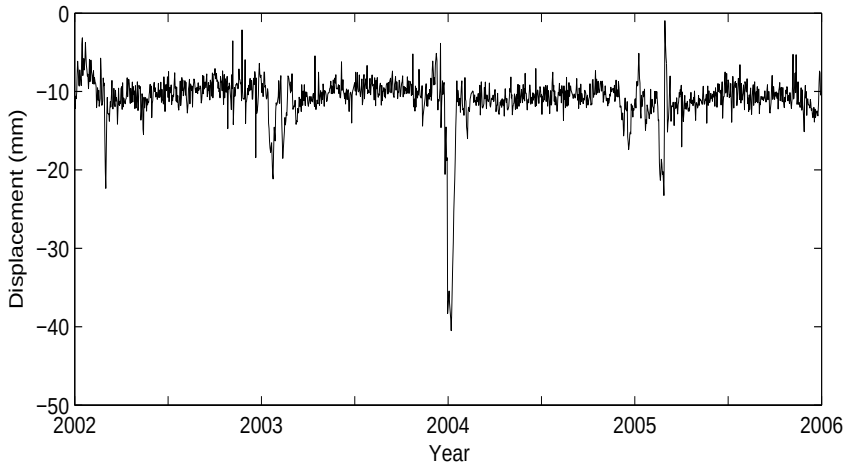

Figure 6.2: GPS Time Series

GPS time series is a time series showing the displacement in North-South (NS), East-West (EW) and in the vertical directions of a GPS station as a function of time. Figure 6.2 shows a GPS time series (BAIE). The signal appears noisy and contains outlier points. In order to analyze the movement of the Earth surface from the GPS time series, these noises and outliers need to be eliminated.

6.7 S Transform Filtering

The CGPS data like most physical data is non-stationary. These signals have time dependent frequency components. The purpose of noise smoothing is to reduce various spurious effects in the data, often of a high-frequency nature, perhaps caused by features such as noise in the data acquisition system, or noise arising as a result of transmission of the data. The data acquired using the GPS techniques are no different. In most cases the data are contaminated by high-frequency noise related to site effects such as monument motion or multipath, as well as longer wavelength regional anthropogenic or seasonal signals, and removing many of these effects remains a challenge.

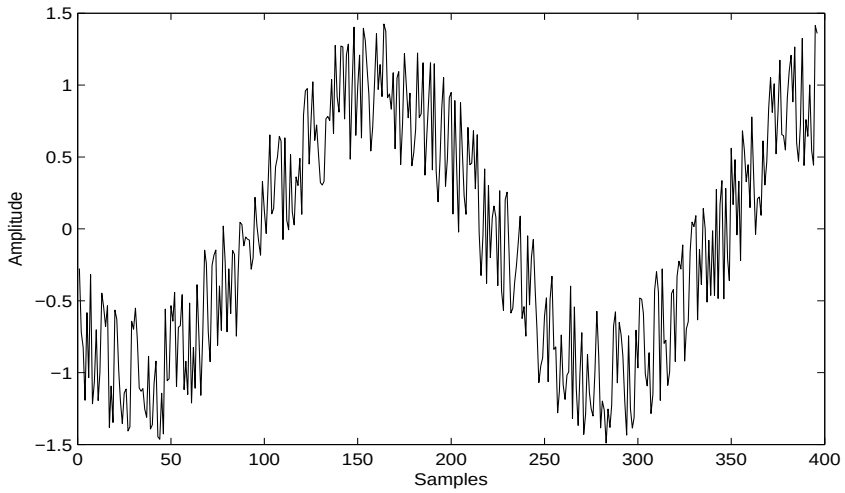

Figure 6.3: Synthetic Time Series

Since the noise in most geophysical signals are non stationary, a time frequency filter need to be used for excision of noise. The S transform filter, discussed in Chapter 5, can be used for the filtering. The filtering process includes a transformation of the time domain signal into the time frequency domain, followed by a time frequency masking operation, which removes the noise components. The TF space obtained after the filtering is inverted

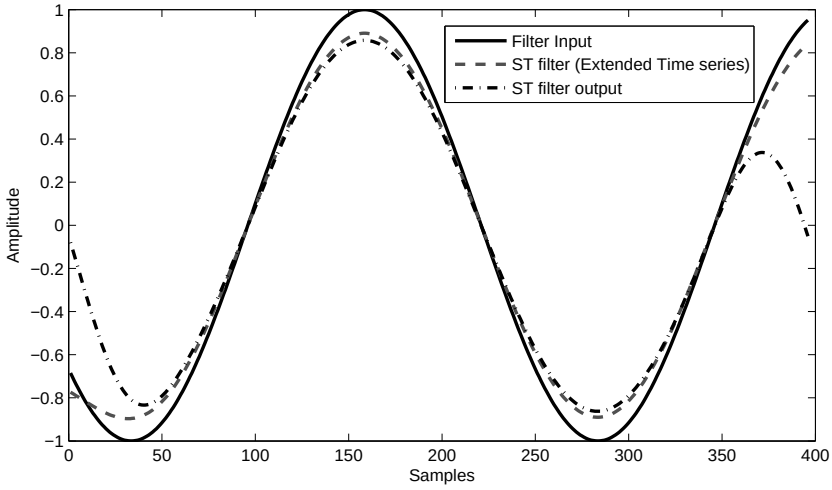

Figure 6.4: Need for Extended S Transform

back to the time domain using Inverse S transform. Before applying to a real GPS signal, the efficiency and correctness of the filtering operation is checked using a synthetic signal. Figure 6.3 shows a synthetic signal, which is a low frequency sinusoidal signal corrupted with Additive White Gaussian Noise (AWGN).

Figure 6.4 shows the S-transform filter output obtained after a low pass filtering. It has been observed that there is a drop in amplitude at the edges of the signal. At the edges, the filtered signal tends to move towards the mean value of the signal. This happens because of the edge effect in S transform as explained in Chapter 3. A possible solution to this problem is an extended S transform filtering approach, which is explained below.

6.7.1 Extended S Transform Filtering

The extended S transform filtering is a crude method of time frequency filtering. A time series of length N is extended to a time series of length $3N$, using the following approach. The original time series is preserved in the extended time series from samples $N+1$ to $2N$. The first sample of the original time series is repeated from samples 1 to N and the last sample is repeated from samples $2N+1$ to $3N$. If f_{org} represents the cutoff frequency for normal S transform low pass filtering of a time series, then the cutoff frequency for the extended time series is taken as three times the cutoff frequency of the original S transform filter (i.e. $3f_{org}$). After the time frequency masking of the extended S transform, an inverse S transform of the S transform plane is used to recover a time

series of length $3N$. The first N and the last N samples of the recovered time series are discarded to get back the filtered N sample time series. The low pass filtering output for the synthetic signal using extended S transform filtering is portrayed in Figure 6.4.

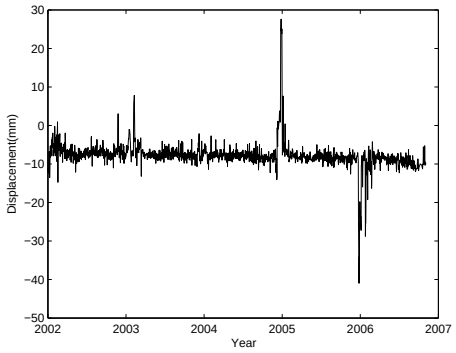

(a) BAIE NS: Original Time Series

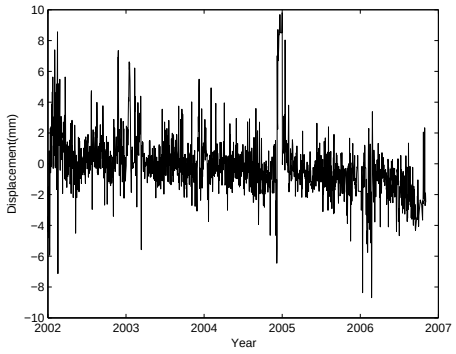

(b) BAIE NS: Time series after removing Outliers

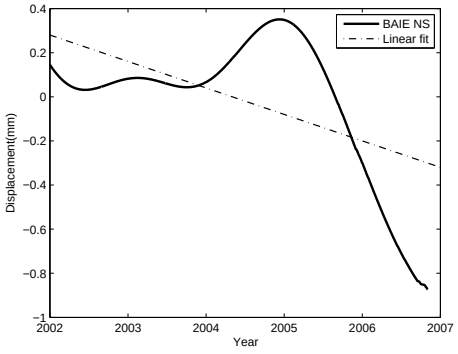

(c) BAIE NS: Filtered Time series

Figure 6.5: BAIE : North South (NS) Time Series

6.8 Analysis and Discussion

The GPS time series for all the 39 GPS stations were filtered using the extended S transform filtering method.

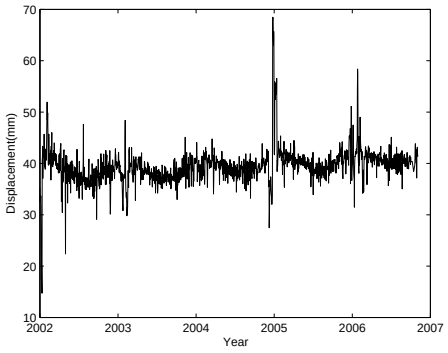

(a) BAIE EW: Original Time Series

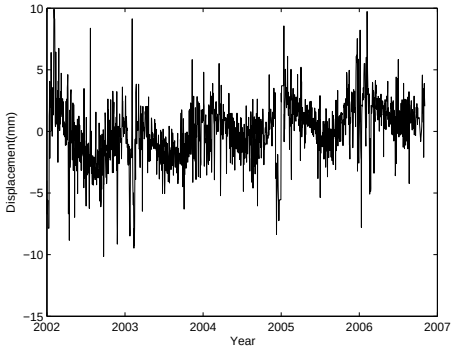

(b) BAIE EW: Time series after removing Outliers

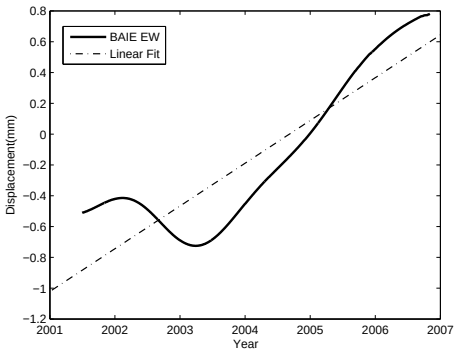

(c) BAIE EW: Filtered Time series

Figure 6.6: BAIE : East West (EW) Time Series

Most of the time series had outliers. An initial pre-processing was done on the time series using statistical methods to remove the obvious outliers in the time series. The time series after removing outliers was fed to the extended S transform filter to remove the high frequency noise components.

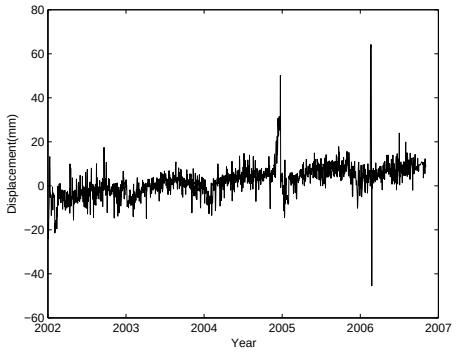

(a) BAIE Vertical: Original Time Series

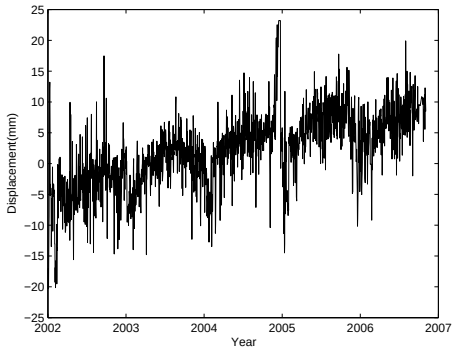

(b) BAIE Vertical: Time series after removing Outliers

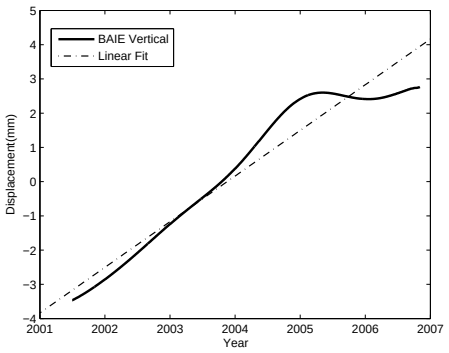

(c) BAIE Vertical: Filtered Time series

Figure 6.7: BAIE : Vertical Time Series

Most of the filter outputs have a linear trend, either in the increasing or decreasing direction. These filtered GPS time series were used as a reference for calculating the velocities. A linear curve was fitted by least squares fitting to the filtered time series, and the slope of that curve represents the velocity of the GPS station movement, which in turn corresponds to the velocity of the Earth's surface. The velocities for all the three directions (North-South, East-West and Vertical) are tabulated in Table 6.1.

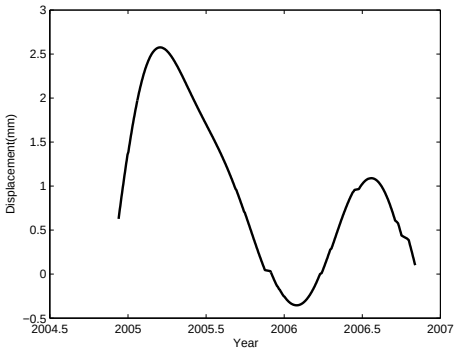

(a) ESCU Vertical: Filtered Time Series

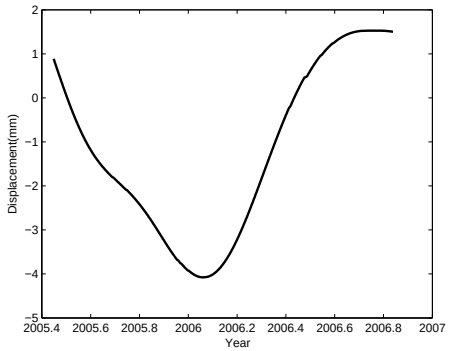

(b) LPOC Vertical: Filtered Time Series

Figure 6.8: Effect of drought at the Great Lakes

The Generic mapping tools (GMT) software was used to represent the velocities as a set of vectors. These velocity vectors plot were plotted on the map of Eastern Canada. Velocity map thus obtained is a plot of the magnitude and direction of the velocity at a particular point on the surface of the earth. Figure 6.9 shows the vertical velocity map for Eastern Canada. The length of the velocity vector indicates the magnitude of the velocity in mm/year and the direction of the vector points to the direction of the motion of the Earth's surface at that GPS station. It can be seen that almost 90 percent of the velocity vectors above a latitude of 44 degrees N are pointing in the vertical direction and most

of the vectors below 44 degree N latitude points towards the downward direction. This velocity map is in tally with the GIA observations for Canada and is a clear indication of a hinge line around 44 degrees N approximately parallel to the St. Lawrence River in the east [40]. The Earth above the hinge line have an uplift and those portions below the hinge line have a subsidence.

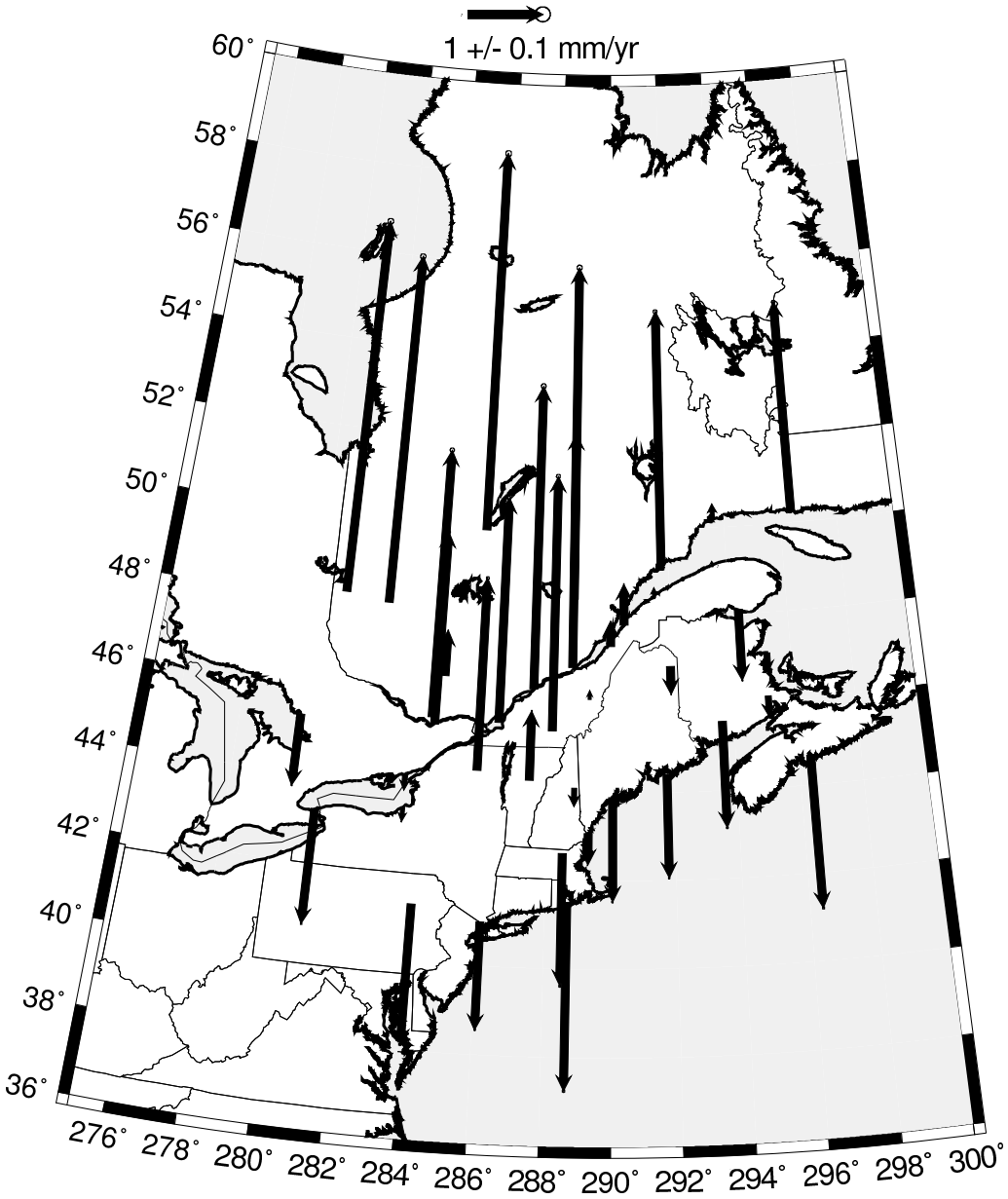

Figure 6.9: Vertical Velocity Map

There exists some stations, which are near the Great Lakes (Lake Michigan, Lake Huron, Lake Erie, Lake Ontario, Lake Superior), which behaved some what different

from the GIA predictions. Figure 6.8 shows the filtered vertical GPS time series for two stations (ESCU, LPOC). The most likely explanation for this discrepancy is the recent persistent drought in the Great Lakes basin. This drought, which began in 1998 and continues, with some fluctuations, through 2007, has significantly lowered the lake levels in Lake Michigan, Lake Huron, and Lake Erie, for example. This could potentially lower the local groundwater levels, which subsequently lower the Earth's surface (GPS Stations).

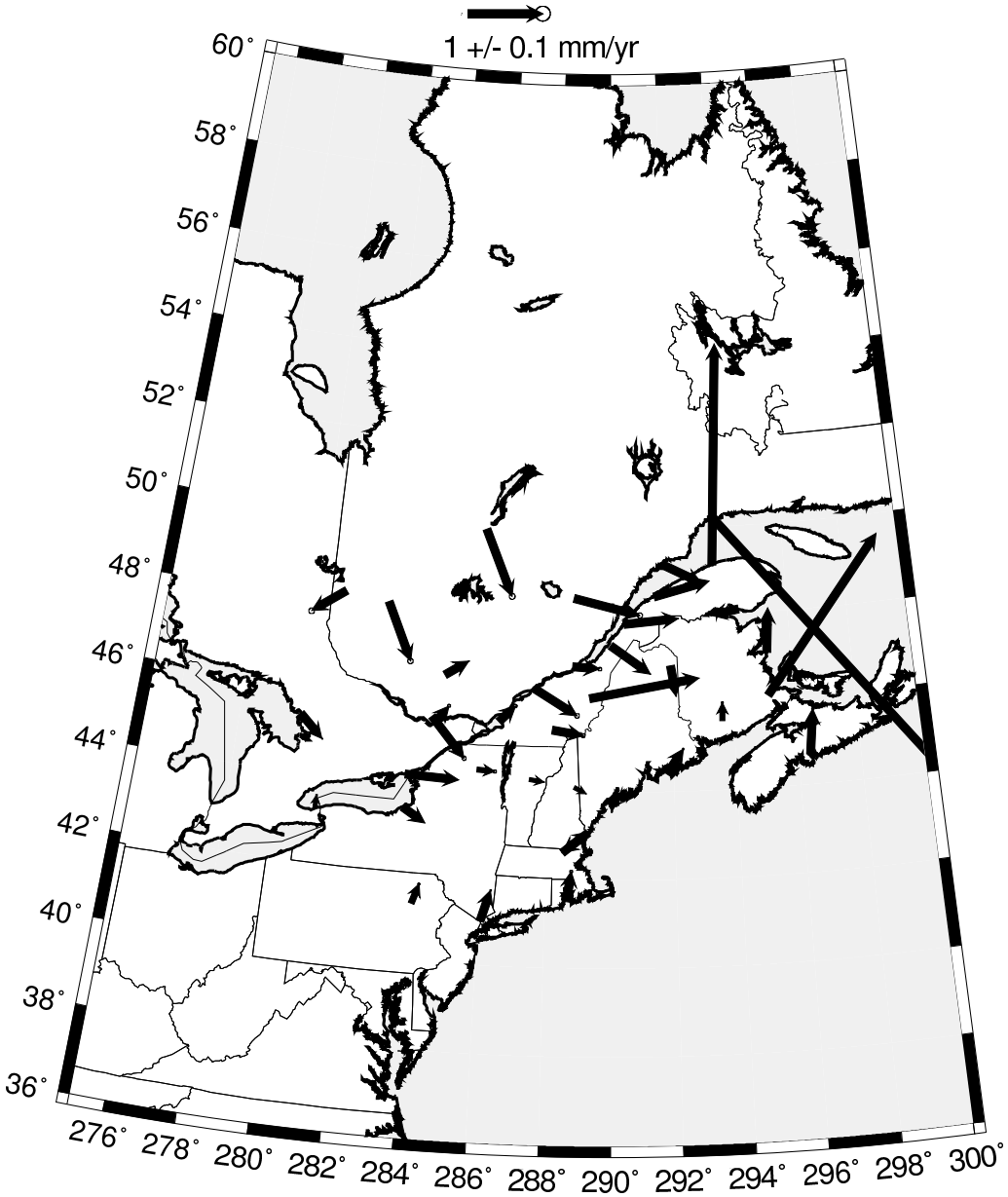

Figure 6.10: Horizontal Velocity Map

Table 6.1: Canada GPS : Velocities

Sl. No.	Station	NS Velocity	EW Velocity	Vertical Velocity	No. of Samples
1	ANNE	2.9504	0.1659	-0.5346	362
2	ATRI	-0.0241	0.3611	1.9431	1892
3	BAIE	-0.2707	0.5357	2.1227	1756
4	BARH	0.3271	0.2263	-0.2411	1858
5	BARN	-0.0806	0.1585	0.0101	1848
6	BRU1	-0.1914	-0.0098	-0.3582	1849
7	CAGS	-0.5344	0.4709	2.0352	1920
8	CAPL	-0.0633	-0.3684	-0.8326	1423
9	CARM	-0.4087	0.0642	-0.9071	753
10	CHIB	-0.8788	0.3860	6.2858	1885
11	CHIC	-0.2211	0.8833	2.9995	1745
12	ESCU	0.5883	0.0525	-0.8959	642
13	GEOR	0.2793	1.4597	-0.5386	1050
14	HLFX	0.5999	0.0773	-1.0641	1734
15	HSTP	0.1561	0.1847	1.0994	1691
16	HULL	0.2439	0.1776	0.5777	1648
17	KNGS	-0.0220	0.7170	-0.1714	1559
18	LAMT	0.4143	0.1187	-0.0085	1559
19	LAUR	0.2034	0.3051	1.7789	691
20	LOUP	0.0687	0.7259	0.9810	608
21	LPOC	-0.3813	0.5299	1.9020	479
22	MCTN	2.0515	1.5832	-3.5152	317
23	MONT	0.2184	0.2132	2.1237	1844
24	NPRI	0.4015	0.0518	-0.2831	1910
25	OSPA	-0.1905	0.3143	0.0638	1460

continued on the next page ...

Canada GPS : Velocities (*continued . . .*)

Sl. No.	Station	NS Velocity	EW Velocity	Vertical Velocity	No. of Samples
26	PARY	-0.3036	0.3250	0.0749	1551
27	POR4	-0.2635	-0.3419	-0.5409	1175
28	PSC1	-0.0125	0.2390	0.8094	1795
29	PWEL	0.0431	0.0190	-0.8270	1576
30	RIMO	0.1941	0.7381	-0.4514	716
31	ROUY	-0.3199	-0.4370	4.6581	1881
32	SEPT	-4.6846	3.8840	0.1307	350
33	SRBK	-0.0664	0.4156	0.7720	1701
34	TRIV	-0.3546	0.5916	1.6194	1768
35	UNB1	0.2406	0.0118	-0.3687	1833
36	VALD	-0.7646	0.3641	5.2948	1690
37	VCAP	-0.0293	0.1958	0.6592	1690
38	WES2	0.2854	0.3503	-0.8876	1753
39	WIL1	0.2626	0.0859	-0.3390	1878

A similar type of velocity map was developed for the horizontal velocities (resultant velocity of the North South and the East West velocities) also. Figure 6.10 depicts the horizontal velocity map. No regular pattern can be seen for the horizontal velocity as observed for the vertical velocities. The horizontal velocity pattern is not definitive, in part due to the short time periods for a significant number of the available stations.

6.9 Conclusion

This chapter introduced S transform filter as a tool for analysis of GPS time series. The crustal velocities derived from the analysis reveal the presence of a post glacial rebound in Eastern Canada. A hinge line was observed as predicted by the GIA models for Eastern Canada.

7

Concluding Remarks

7.1 Conclusion

Fourier transforms are limited to the analysis of stationary time series. Time frequency analysis techniques were developed to overcome this limitation. The Short Time Fourier transform and the Wavelet transforms have several disadvantages. This led to the development of the S transform, which is a hybrid of both the transforms. The original S transform developed by Stockwell, Mansinha and Lowe suffered from poor time frequency resolution. This thesis introduced a modified S transform with better time frequency resolution. The improvement is achieved through the introduction of a new scaling rule for the S transform Gaussian window.

The S transform was used in Chapter 4 for the analysis of business cycles. The analysis revealed the presence of short term cycles in the stock market time series, which were not visible in the time domain. The business cycles could be used for forecasting economic upswings and depressions. The analysis of global oil price brought out the occurrence of short term cycles in oil price that repeats during the times of war.

Chapter 5 presented a new time frequency filtering approach. Image processing techniques were combined with S transform time-frequency representation to design filters that can remove even time limited and band limited noise through a two stage filtering process. The filter method appears robust within a wide range of background noise levels. More work needs to be done to make this method operate for highly noisy signals. The filtering technique was applied in Chapter 6 for the detection of post glacial rebound in Eastern Canada. The results obtained are in close agreement with the post glacial rebound models available.

7.2 Scope for Future Work

Even though the time frequency resolution obtained in S transform and the modified S transform proposed in this thesis are better than Short Time Fourier Transform, it is still far from ideal. Heisenberg's uncertainty principle offers a restriction on the achievable time frequency resolution. Much remains to be done to achieve perfect time frequency resolution. The gradient of the local variance can be used to calculate the frequency trend of a time series, but it requires refinement and the development of a mathematical basis. S transform can be applied for the analysis of time series from diverse areas. Even though business cycles were analyzed in detail, more study is necessary on its relationship to various other factors that affect the GDP of a country. The interest rate is one such

factor that may be analyzed.

The S transform of a time series of length N produces an S matrix of size $N \times N/2$. Each point in the S matrix is a complex number. Thus the S transform requires a good amount of memory for storage of the 2D complex matrix. As the Gaussian window gets wider in the frequency domain, in the higher frequency range, the incremental width of the Gaussian window with an increase in frequency is often less than one sample interval. This property of the window can be used to develop a compact S transform, which will produce a sparse matrix as compared to the $N \times N/2$ complex matrix produced by normal S transform. Inverting techniques need to be developed to recover the original S transform from the compact S transform.

The S transform has a frequency step computation procedure. i.e. The $N/2$ frequency voices are computed separately one at a time. This increases the computation time of the S transform. The S transform computation time can be improved by making use of the properties of a Toeplitz matrix, which is a matrix in which each descending diagonal from left to right is constant. Time Variance (TV) is another possible candidate for analysis of a time series. The time variance analysis produces 2D representation of local variance with time. TV analysis is expected to reveal more detailed information from a time series.

Bibliography

[1] Box G. E. P. and Jenkins G., *Time Series Analysis: Forecasting and Control*, Holden-Day, 1976.

[2] Stockwell R. G. , *S–Transform Analysis of Gravity Wave Activity*, Ph.D. Dissertation, Dept. of Physics and Astronomy, The University of Western Ontario, London, Ontario, Canada, 1999.

[3] Michael R. Portnoff, *Time–Frequency Representation of Digital Signals and Systems Based on Short-Time Fourier Analysis*, IEEE Transactions On Acoustics, Speech, And Signal Processing, Vol. Asp–28, No. 1,(1980), pp:55–69.

[4] Ingrid Daubechies, *The Wavelet Transform, Time–Frequency Localization and Signal Analysis*, IEEE Trans. On Information Theory, Vol.36, No. 5, (1990), pp:961–1005.

[5] Stockwell R.G, Mansinha L and Lowe RP *Localisation of the complex spectrum: the S transform*, IEEE Trans. Signal Processing, 44, (1996), pp:998-1001.

[6] Eramian M., Schincariol R., Stockwell R., Lowe R. and Mansinha L., *Review of applications of 1D and 2D S–transforms*, Wavelet Applications IV 3078,(1996), pp:558–568.

[7] Eramian M., Schincariol R., Mansinha L. and Stockwell, R., *Generation of aquifer heterogeneity maps using two–dimensional spectral texture segmentation techniques*, Mathematical Geology 31, (1999), pp:327–348.

[8] Rakovi P. , Sejdic E., Stankovi L.J. and Jiang J., *Time–Frequency Signal Processing Approaches with Applications to Heart Sound Analysis*, Computers in Cardiology, Vol:33, (2006), pp:197–200.

[9] Assous S., Humeau A., Tartas M., Abraham P., and LHuillier J., *S–transform applied to laser doppler flowmetry reactive hyperemia signals*, IEEE Trans. Biomed. Eng. 53, (2006), pp:1032-1037.

[10] Dash P.K., Samantaray S.R., Panda G. and Panigrahi B.K., *Power transformer protection using S-transform with complex window and pattern recognition approach*, IET Gener. Transm. Distrib., Vol. 1, (2007), pp:278–286.

[11] Dash P. K., Panigrahi B. K., Sahoo D. K., and Panda G., *Power Quality Disturbance Data Compression, Detection, and Classification Using Integrated Spline Wavelet and S-Transform*, IEEE Transactions On Power Delivery, Vol. 18, (2003), pp:595–600.

[12] Chien-Chun Huang, Sheng-Fu Liang, Ming-Shing Young and Fu-Zen Shaw, *A novel application of the S–transform in removing powerline interference from biomedical signals*, Physiological Measurement, 30, (2009), pp: 13–27.

[13] Stockwell R.G., *Why use the S-Transform?*, AMS Pseudo–differential operators: partial differential equations and time–frequency analysis, Vol. 52,(2007), pp:279–309.

[14] McFadden P. D., Cook J. G. and Forster L. M., *Decomposition of gear vibration signals by the generalized S-transform*, Mechanical Systems and Signal Processing, vol. 13, no. 5, (1999), pp:691–707.

[15] Robert Pinnegar C. and Lalu Mansinha, *The S–transform with windows of arbitrary and varying shape*, Geophysics, Vol. 68, No. 1, (2003), pp:381-385.

[16] Mansinha L., Stockwell R. G. and Lowe R. P., *Pattern analysis with two-dimensional spectral localisation: Applications of two-dimensional S-transforms*, Physica A, 239, (1997), pp:286-295.

[17] Robin Bade and Michael Parkin, *Foundations of Economics*, 4th edition, Addison Wesley, 2007.

[18] Christina D. Romer, *Business Cycles*, The Concise Encyclopedia of Economics,Library of Economics and Liberty, 2008.

[19] Zarnowitz V., *Business Cycles: Theory, History, Indicators, and Forecasting*, National Bureau of Economic Research, Studies in Business, 1992.

[20] Joseph A. Schumpeter, *Business Cycles: A theoretical, historical and statistical analysis of the Capitalist process*, 1939.

[21] Yogo and Motohiro, *Measuring Business Cycles: A Wavelet Analysis of Economic Time Series*, Economics Letters, Vol. 100, No. 2, (2008), pp:208–212.

[22] Ayhan Kose M. , Christopher Otrok and Charles H. Whiteman1, *Understanding the Evolution of World Business Cycles*, IMF Working Paper, (2005), pp:1–36.

[23] Walter C. Labys, *Globalization, Oil Price Volatility, and the US Economy*,Research Paper, West Virginia University, (2006), pp:21–26.

[24] Antonia Papandreou-Suppappola, *Applications in Time-Frequency Signal Processing*, CRC Press, 2003.

[25] Saleh B.E.A. and Subotic N.S., *Time–variant filtering of signals in the mixed time–frequency domain*, IEEE Trans. ASSP 33, (1985), pp:1479-1485.

[26] Pinnegar C.R., *Time-frequency and time-time filtering with the S-transform and TT-transform*, Digital Signal Processing 15, (2005), pp:604-620.

[27] Schimmel M. and Gallart J., *The Inverse S-Transform in filters with Time–Frequency Localization*, IEEE Trans. Signal Processing 55 (11), (2005), pp:4417-4422.

[28] R. M. Haralick ,S. R. Sternberg and X. Zhuang, *Image analysis using mathematical morphology*, IEEE Transactions on Pattern Analysis and Machine Intelligence,9,(1987), pp: 532–550.

[29] Chris Rizos, *Introduction to GPS*, Lecture Notes – University of New South Wales, 1999.

[30] Jay Farrell and Matthew Barth ,*The global positioning system and inertial navigation*, McGraw-Hill, 1999.

[31] Sergey V Samsonov, *Integration of differential INSAR and GPS measurements for studying of surface deformation*, Ph.D Thesis, University of Western Ontario, 2007.

[32] Tiampo K. F., Dawit Assefa, Fernandez J., Mansinha L. and Rasmussen H.,*Postseismic Deformation Following the 1994 Northridge Earthquake Identified Using the Localized Hartley Transform Filter*, Pure Applied Geophysics. 165, (2008), pp:1577-1602.

[33] Andrea Donnellan, Jay W. Parker and Gilles Peltzer, *Combined GPS and InSAR Models of Postseismic Deformation from the Northridge Earthquake*, Pure appl. geophys., Vol-159,(2002), pp:2261-2270.

[34] Kuo-En Ching, Ruey-Juin Rau , Jian-Cheng Lee and Jyr-Ching Hu, *Contemporary deformation of tectonic escape in SW Taiwan from GPS observations, 19952005*, Earth and Planetary Science Letters 262, (2007), pp: 601-619.

[35] Reddy C. D. and Sanjay K. Prajapati, *GPS measurements of postseismic deformation due to October 8, 2005 Kashmir earthquake*, Springer J Seismol, (2008).

[36] Mitrovica, J.X., G.A. Milne and J.L. Davis, *Glacial isostatic adjustment on a rotating earth*, Geophysical Journal International 147, (2001), pp: 562-578.

[37] Peltier W.R., *Postglacial variations in the level of the sea: implications for climate dynamics and solid–earth geophysics*, Reviews of Geophysics 36, (1998), pp: 603-689.

[38] Sella G.F., Stein S., Dixon T.H., Craymer M., James T.S., Mazzotti S. and Dokka R.K, *Observation of glacial isostatic adjustment in stable North America with GPS*, Geophysical Research Letters 34, (2007), L02306.

[39] Johansson J.M., *Continuous GPS measurements of postglacial adjustment in Fennoscandia*, Journal of Geophysical Research 107, (2002), pp: 21–57.

[40] Peltier W. R. , *Global glacial isostatic adjustment: Palaeogeodetic and space–geodetic tests of the ICE-4G (VM2) model*, J. Quat. Sc., 17, (2002), pp:491–510.